Exome-wide rare variant analysis identifies TUBA4A mutations associated with familial ALS

Smith, Bradley N; Morrison, Karen; Pall, Hardev; Ticozzi, Nicola; Fallini, Claudia; Gkazi, Athina Soragia; Topp, Simon; Kenna, Kevin P; Scotter, Emma L; Kost, Jason; Keagle, Pamela; Miller, Jack W; Calini, Daniela; Vance, Caroline; Danielson, Eric W; Troakes, Claire; Tiloca, Cinzia; Al-Sarraj, Safa; Lewis, Elizabeth A; King, Andrew

DOI:
10.1016/j.neuron.2014.09.027

Document Version
Peer reviewed version

Citation for published version (Harvard):
Smith, BN, Morrison, K, Pall, H, Ticozzi, N, Fallini, C, Gkazi, AS, Topp, S, Kenna, KP, Scotter, EL, Kost, J, Keagle, P, Miller, JW, Calini, D, Vance, C, Danielson, EW, Troakes, C, Tiloca, C, Al-Sarraj, S, Lewis, EA, King, A, Colombrita, C, Pensato, V, Castellotti, B, de Belleroche, J, Baas, F, ten Asbroek, ALMA, Sapp, PC, McKenna-Yasek, D, McLaughlin, RL, Polak, M, Asress, S, Esteban-Pérez, J, Muñoz-Blanco, JL, Simpson, M, van Rheenen, W, Diekstra, FP, Lauria, G, Duga, S, Corti, S, Cereda, C, Corrado, L, Sorarù, G, Williams, KL, Nicholson, GA, Blair, IP, Dion, PA, Leblond, CS, Rouleau, GA, Hardiman, O, Veldink, JH & SLAGEN Consortium 2014, 'Exome-wide rare variant analysis identifies TUBA4A mutations associated with familial ALS', *Neuron*, vol. 84, no. 2, pp. 324-31. https://doi.org/10.1016/j.neuron.2014.09.027

Exome-Wide Rare Variant Analysis Identifies TUBA4A Mutations Associated with Familial ALS

Bradley N. Smith[1,30], Nicola Ticozzi[2,3,30], Claudia Fallini[4,30], Athina Soragia Gkazi[1,30], Simon Topp[1,30], Kevin P. Kenna[4,5], Emma L. Scotter[1], Jason Kost[4,6], Pamela Keagle[4], Jack W. Miller[1], Daniela Calini[2,3], Caroline Vance[1], Eric W. Danielson[4], Claire Troakes[1], Cinzia Tiloca[2], Safa Al-Sarraj[1], Elizabeth A. Lewis[4], Andrew King[1], Claudia Colombrita[2,3], Viviana Pensato[7], Barbara Castellotti[7], Jacqueline de Belleroche[8], Frank Baas[8], Anneloor LMA ten Asbroek[9], Peter C. Sapp[4], Diane McKenna-Yasek[4], Russell L. McLaughlin[5], Meraida Polak[10], Seneshaw Asress[10], Jesús Esteban-Pérez[11], José Luis Muñoz-Blanco[12], Michael Simpson[13], SLAGEN Consortium, Wouter van Rheenen[14], Frank P. Diekstra[14], Giuseppe Lauria[15], Stefano Duga[16], Stefania Corti[3,17], Cristina Cereda[18], Lucia Corrado[19], Gianni Sorarù[20], Karen E. Morrison[21,22], Kelly L. Williams[23], Garth A. Nicholson[23,24], Ian P. Blair[23], Claire S. Leblond[25], Guy A. Rouleau[25], Orla Hardiman[5], Jan H. Veldink[14], Leonard H. van den Berg[14], Ammar Al-Chalabi[26], Hardev Pall[27], Pamela J. Shaw[28], Martin R. Turner[29], Kevin Talbot[29], Franco Taroni[7], Alberto García-Redondo[11], Zheyang Wu[6], Jonathan D. Glass[10], Cinzia Gellera[7], Antonia Ratti[2,3], Robert H. Brown Jr.[4], Vincenzo Silani[2,3,31], Christopher E. Shaw[1,31], John E. Landers[4,30,31,*]

[1]Centre for Neurodegeneration Research, King's College London, Department of Clinical Neuroscience, Institute of Psychiatry, London SE5 8AF, UK.

[2]Department of Neurology and Laboratory of Neuroscience, IRCCS Istituto Auxologico Italiano, Milan 20149, Italy.

[3]Department of Pathophysiology and Transplantation, 'Dino Ferrari' Center - Università degli Studi di Milano, Milan 20122 Italy.

[4]Department of Neurology, University of Massachusetts Medical School, Worcester, Massachusetts 01605, USA.

[5]Academic Unit of Neurology, Trinity Biomedical Sciences Institute, Trinity College Dublin, Dublin, Republic of Ireland.

[6]Worcester Polytechnic Institute, Worcester, MA 01609, USA.

[7]Unit of Genetics of Neurodegenerative and Metabolic Diseases, Fondazione IRCCS Istituto Neurologico 'Carlo Besta', Milan 20133, Italy.

[8]Neurogenetics Group, Division of Brain Sciences, Hammersmith Hospital Campus, Burlington Danes Building, Du Cane Road, London W12 0NN.

[9]Department of Genome analysis and Neurogenetics, Academic Medical Centre, Amsterdam, The Netherlands.

[10]Department of Neurology, Emory University, Atlanta, GA 30322, USA.

[11]Unidad de ELA, Instituto de Investigación Hospital 12 de Octubre de Madrid, SERMAS, and Centro de Investigación Biomédica en Red de Enfermedades Raras (CIBERER U-723), Madrid, Spain.

[12]Unidad de ELA, Instituto de Investigación Hospital Gregorio Marañón de Madrid, SERMAS, Spain.

[13]Department of Genetics and Molecular Medicine, King's College London. Tower Wing, Guy's Hospital, London SE1 7EH, UK.

[14]Department of Neurology, Brain Center Rudolf Magnus Institute of Neuroscience, University Medical Centre Utrecht, 3508 GA Utrecht, The Netherlands.

[15]Headache and Neuroalgology Unit, Fondazione IRCCS Istituto Neurologico 'Carlo Besta', Milan 20133, Italy.

[16]Department of Medical Biotechnology and Translational Medicine - Università degli Studi di Milano, Milan, Italy.

[17]Neurology Unit, IRCCS Foundation Ca' Granda Ospedale Maggiore Policlinico, Milan 20122, Italy.

[18]Experimental Neurobiology Laboratory, IRCCS 'C. Mondino' National Neurological Institute, 27100 Pavia, Italy.

[19]Department of Medical Sciences, 'A. Avogadro' University of Eastern Piedmont, Novara, Italy.

[20]Department of Neurosciences, University of Padova, Padova, Italy.

[21]School of Clinical and Experimental Medicine, College of Medical and Dental Sciences, University of Birmingham, UK.

[22]Queen Elizabeth Hospital, University Hospitals Birmingham NHS Foundation Trust UK.

[23]Australian School of Advanced Medicine, Macquarie University, Sydney, NSW 2109, Australia.

[24]Northcott Neuroscience Laboratory, ANZAC Research Institute, Sydney, NSW 2139, Australia.

[25]Montreal Neurological Institute, Department of Neurology and Neurosurgery, McGill University, Montreal, Quebec, Canada.

[26]Department of Clinical Neuroscience, Medical Research Council Centre for Neurodegeneration Research, Institute of Psychiatry, King's College London, London, UK.

[27]School of Clinical and Experimental Medicine, College of Medical and Dental Sciences, The University of Birmingham, Birmingham, UK.

[28]Sheffield Institute for Translational Neuroscience, University of Sheffield, Sheffield, UK.

[29]Nuffield Department of Clinical Neurosciences, University of Oxford, UK.

[30,31]These authors contributed equally to this work.

* Correspondence: john.landers@umassmed.edu.

RUNNING TITLE: Identification of TUBA4A Mutations in ALS

SUMMARY

Exome sequencing has proven to be an effective strategy for identifying human disease genes. However, this methodology can be difficult in late-onset diseases where limited availability of DNA from informative family members often prohibits comprehensive segregation analysis. To overcome this limitation, we performed a exome-wide rare

variant burden analysis of 363 index cases with familial ALS (FALS). The results revealed an excess of patient variants within *TUBA4A*, the gene encoding the Tubulin, Alpha 4A protein. Analysis of a further 272 FALS cases and 5510 internal controls confirmed the over representation as both statistically significant and replicable. Functional analyses revealed that TUBA4A mutants lead to a destabilized microtubule network and diminished repolymerization capability. Taken together, these results further emphasize the role of cytoskeletal defects in ALS. Moreover, they demonstrate the power of gene based rare variant analyses in situations where causal genes cannot be identified through traditional segregation analysis.

HIGHLIGHTS

- Mutations in tubulin, alpha 4A (*TUBA4A*) are associated with familial ALS
- TUBA4A mutants act as dominant negatives to alter microtubule dynamics and stability
- Further evidence supports a major role of cytoskeletal defects in ALS pathogenesis
- Rare variant analysis of index familial cases can identify human disease genes

INTRODUCTION

The identification of mutations for human disorders is critical for our understanding of their pathogenesis. Over the past few years, numerous studies have successfully used exome sequencing to rapidly identify novel disease genes. Despite these advances, this approach is still limited by the fact that each individual harbors hundreds of rare variants, thus requiring DNA from multiple affected individuals from an affected family

for this method to be successful. Unfortunately, for many diseases the DNA collection of multiple affected samples from the same family can be difficult. This is especially true for familial amyotrophic lateral sclerosis (FALS), a late-onset, rapidly progressive neurodegenerative disease. As such, there is a need to develop approaches to use individual affected cases to identify disease genes. Exome-wide rare variant analysis has been proposed as a promising alternative strategy for disease gene identification (Panoutsopoulou et al., 2013; Stitziel et al., 2011). By this approach, the total number of gene variants seen among cases is compared to that seen among controls. Threshold minor allele frequency and possibly functional significance filters are implemented to prevent statistical noise from common or other neutral variants masking true gene associations. Importantly, although an abundance of variants in cases suggests the presence of pathogenic mutations, an associated variant set will still likely include neutral variants in both cases and controls. Given that these methods do not rely on related samples, we decided to use this approach to identify novel causative genes for familial ALS.

RESULTS

We performed exome sequencing on a discovery cohort of 363 index cases (i.e. one affected sample per family) collected from 6 countries (Ireland, Italy, Netherlands, Spain, UK, US) (see Table S1 available online) devoid of causative mutations/ repeat expansions in known ALS genes (*SOD1*, *C9orf72*, *TARDBP*, *FUS*, *PFN1*, *UBQLN2*, *OPTN*, *VCP*, *ANG)*. An average of 3.2×10^9 target bases were sequenced per sample to an average depth of 90.4X (Tables S2 and S3). Control exome data included 4300

European Americans available through the NHLBI's Exome Variant Server (EVS)(Tennessen et al., 2012), and 31 internally sequenced samples. As proof of principle, we spiked our sample set with 9 FALS exomes from individuals with known causative mutations (6 in SOD1 and 3 in VCP). The analysis was restricted to the 12,487 genes fulfilling all quality control filters and to variants either predicted to be damaging using PolyPhen-2 or resulting in a stop gain/loss. Variants were also only considered if they exhibited minor allele frequencies less than 0.04% in keeping with previously reported ALS mutations (Chio et al., 2012; Kenna et al., 2013) (Supplemental Experimental Procedures) and the significance of disease associations following multiple test correction ($P_{corrected}$) were calculated using permutation procedures (Kiezun et al., 2012). Strong signals of disease association were observed across *SOD1* (6 cases [1.6%] vs 0 controls, $P=5.5 \times 10^{-8}$, $P_{corrected}=6.2 \times 10^{-4}$) and *VCP* (3 cases [0.8%] vs 0 controls, $P=1.1 \times 10^{-4}$, $P_{corrected}=0.73$) (Figure 1A and Figure S1). Excluding *SOD1*, the top hit from our analysis was *TUBA4A*, encoding the Tubulin, Alpha 4A protein (4 cases [1.1%] vs 0 controls, $P=9.1 \times 10^{-6}$, $P_{corrected}=0.09$). The gene is well covered by EVS confirming that the *P*-value was not inflated due to poor control sequencing (Figure S2). *TUBA4A* also exhibited associations of similar significance when alternative bioinformatic tools were used to identify putatively damaging disease variants (SIFT, GERP, MutationTaster, phyloP). Furthermore, *TUBA4A* ranked 1st or 2nd in all tests (Table S4 and Figure S3) while no other gene ranked in the top 10 hits for all 5 tests. Although *TUBA4A* was the most consistent hit, our strategy revealed several other strong candidate genes for FALS (Figure 1A, Table S4, Supplemental Files) including *MATR3*, responsible for distal myopathy 2 and recently identified by another group as

causative for FALS (Johnson et al., 2014). Other candidate genes include *STK24*, a mediator of oxidative-stress-induced cell death, and *LRRFIP1*, a GC-rich DNA/double stranded RNA binding protein (UniProtKB). Based on these results, we further investigated *TUBA4A* as a candidate gene associated with FALS.

Exome sequencing revealed a total of 5 non-synonymous *TUBA4A* changes, all of which localized to exon 4 and confirmed by Sanger sequencing (Table S5 and Figure S4). None of these mutations were observed in the 4300 European American EVS controls and all occurred within highly conserved positions (Figure 1B). The mutations included 2 missense changes in the same residue (R320C/H) and a nonsense mutation (W407X) removing the last 41 amino acids. This C-terminal region contacts the tubulin beta subunit as well as the motor domain of kinesins and other microtubule-associated proteins (Howes et al., 2014; Liu et al., 2012) (Figure 1C). Additional missense changes included a R215C and A383T mutation. PolyPhen-2 predicted 4 of the 5 mutations to be deleterious (Table S6). In contrast, only three non-synonymous changes were observed in the 4300 EVS controls and none were predicted to be damaging. No relatives of the affected patients were available to test segregation.

To further evaluate *TUBA4A* as a causative ALS gene, an independent replication cohort comprising a further 272 index FALS cases and 5510 internal European American controls was sequenced for rare damaging exon 4 variants (Table S7). Reimplementation of the variant filtering strategies employed during the discovery analysis and subsequent testing using Fisher's exact method again revealed a significant excess of mutation carriers among patients (2 cases [0.65%] vs 2 controls

[0.04%], P=1.5x10^{-2}). A combined analysis of the discovery and replication cohorts resulted in a statistically significant over abundance of rare variants after multiple test correction (OR=36 [95% CI:10-210], P=4.3x10^{-7}, $P_{corrected}$=4.2x10^{-3}). Mutation carriers observed among patients from the replication cohort included a single carrier of a T145P variant and a single carrier of a K430N variant. Screening of an affected parent and unaffected sibling confirmed the expected segregation pattern in the case of T145P (Figure S5). The K430N variant was not detected in an affected first cousin of the sequenced proband (Figure S5) suggesting that this is either a neutral polymorphism, as is often observed in rare variant analyses, or the two affected family members represent phenocopies. Variants identified in the control cohort included E386K and G365E substitutions but no variant detected in FALS patients from either the discovery or replication cohorts. Sequencing of the entire coding region in 1355 sporadic ALS cases also identified a G43V mutation in a single sample (Table S5). This variant was predicted to be benign by PolyPhen-2 and detected within 1 control from the internal replication panel. No *TUBA4A* mutations were identified in 131 ALS samples (89 FALS and 42 SALS) with known causative mutations/repeat expansions (Table S8).

All patients carrying *TUBA4A* mutations had spinal-onset, classical ALS, with upper and lower motor neuron signs. Two cases developed during the course of the disease a cognitive decline of frontal type, consistent with a diagnosis of frontotemporal dementia (FTD) and another had a first-degree relative with FTD (Figure S5 and Table S9). Screening of samples analyzed by the 1000Genome project (1053 samples) and 2200 African Americans from the EVS revealed the A383T mutation within a single individual of African ancestry. Therefore, with the exception of A383T and G43V, the set of

observed patient variants were not detected within a total of 13,023 control samples (Table S10).

TUBA4A Mutants Display Altered Incorporation Into Microtubules

Since several causative ALS proteins have been shown to form insoluble inclusions in postmortem brain tissues and in cell culture, we investigated the ability of TUBA4A mutants identified in our initial analysis to aggregate by expressing HA-tagged TUBA4A constructs in primary motor neurons (PMNs) and HEK293 cells. Interestingly, the W407X mutant did not incorporate into the microtubule network and formed small ubiquitinated cytoplasmic inclusions in ~40% of transfected PMNs and ~85% of transfected HEK293 cells (Figure 2A,B; Figure S6 and S7). Immunohistochemistry of brain and spinal cord tissue from sporadic ALS cases (without mutations) yielded a clear staining of the perikarya and neuropil region in both the spinal cord and motor cortex, however no TUBA4A aggregates were identified (Figure S8). No coaggregation was observed in cells co-expressing an aggregation-prone TDP-43 C-terminal fragment and wild-type TUBA4A (Figure S9). While the other TUBA4A mutants formed cytoplasmic inclusions in 10-30% of transfected HEK293 cells (data not shown), no aggregation was observed in PMNs. However, subtle alterations in their cytoplasmic distribution were observed, such as a more diffuse cytoplasmic staining compared to the wild-type protein, which was mainly incorporated into the microtubule network (Figure 2A). We thus investigated the ability of mutant TUBA4A to efficiently form microtubules using a cell-free system to quantify the incorporation of the mutant TUBA4A into alpha/beta tubulin dimers (Cleveland et al., 1978; Jaglin et al., 2009; Tian

et al., 2010). Each mutant was subjected to *in vitro* translation in rabbit reticulocyte lysate that contains all components needed to form tubulin dimers. The products were then analyzed by non-denaturing gel electrophoresis to measure incorporation of the translated recombinant protein into tubulin dimers. SDS-gel electrophoresis was performed in parallel to control for equal protein synthesis and loading. Interestingly, the TUBA4A^{W407X} protein yielded no discernible dimers, while the A383T and both R320 mutants displayed significantly lower levels of assembly relative to the wild-type protein (Figure 2C,D). The other mutants did not differ from the control, save for a small but reproducible migration difference for TUBA4A^{R215C} protein. In parallel, we then tested the incorporation of mutant TUBA4A into microtubules in cultured cells. We chose primary astroglial cells for the HA-tagged TUBA4A transfections, as they have a large cytoplasm and a relatively long cell cycle that result in an extensive and stable microtubule network. We performed an unbiased analysis of the cytoskeletal incorporation of HA-tagged TUBA4A constructs by applying a circularity filter to the images in order to discriminate between filamentous and diffuse granular staining (Supplemental Experimental Procedures). The ratio between the fluorescence intensities of the filamentous versus overall staining, ranging from 1 to 0, was used to categorize each cell as normal (1-0.75), mild (0.75-0.5), moderate (0.5-0.25), or severe (0.25-0) phenotype (Figure 2E,F and Figure S10). The wild-type HA-tagged TUBA4A protein yielded nearly 70% of cells displaying a high level of microtubule incorporation (Figure 2E,F). In contrast, several of the mutants displayed an altered incorporation into microtubules. In particular, the W407X yielded the most dramatic effect with an absence of tagged protein in the microtubule network and the presence of multiple aggregate-like

inclusions. The R320C/H, A383T and R215C mutants all displayed a significantly different distribution relative to the wild-type, but no differences were detected for the G43V protein.

TUBA4A Mutants Disrupt Microtubule Dynamics and Stability Through a Dominant-Negative Mechanism

We next determined whether TUBA4A mutants affected microtubule assembly dynamics by testing the ability of TUBA4A-transfected COS7 cells to recover after transient microtubule depolymerization following treatment with 10 μM nocodazole (Figure 3)(Gilissen et al., 2011; Tian et al., 2007; 2010). For this assay, the wild-type, R320C, and W407X proteins were compared, as these mutants displayed an intermediate and severe phenotype respectively in the previous experiments. While ~80% of cells transfected with TUBA4A^{WT} formed centrosomes positive for the HA-tagged TUBA4A protein within 5 minutes of nocodazole removal, only ~20% of TUBA4A^{R320C}-transfected cells formed a new microtubule network containing the mutant protein at 15 minutes. Interestingly, the expression of mutant TUBA4A also impaired the ability of the endogenous protein to form microtubules, as only 50% of the cells contained TUBA4A-positive microtubules after 15 minutes, compared to ~90% in wild-type transfected cells (Figure 3A,B and Figure S11). Similar results were also observed in cells containing TUBA4A^{W407X}–positive aggregates. On the contrary, cells expressing the TUBA4A^{W407X} mutant without the presence of aggregates did not display any defect in the rate of microtubule repolymerization (Figure 3C,D). These results suggest that mutant TUBA4A by incorporating into the microtubules may disrupt their dynamics through a dominant-negative mechanism.

To pursue this hypothesis further, we investigated whether TUBA4A mutants would influence the overall stability of the microtubule network. Primary motor neurons were transfected with wild-type and mutant TUBA4A constructs, permeabilized with 0.1% Triton X-100 to extract all soluble proteins before fixation and immunostained for HA-TUBA4A and β-tubulin. Under these conditions, the microtubule cytoskeleton was largely preserved in wild-type transfected neurons, whereas each of the missense mutants resulted in decreased HA-TUBA4A and β-tubulin immunofluorescence (Figure 4A-C). The TUBA4A^{W407X} mutant yielded no cells with visible HA staining (data not shown) indicating a complete failure of incorporation into the network. Furthermore, the levels of α-tubulin acetylation, which have been shown to correlate with increased microtubule stability (Matsuyama et al., 2002; Piperno et al., 1987; Wu et al., 2012), were significantly reduced in mutant TUBA4A-expressing motor neurons (Figure 4D,E and Figure S12). Interestingly, the G43V mutation, which is uniquely localized to the protein N-terminus, did not impair tubulin acetylation, suggesting that defective binding of the acetyl-transferase αTAT1 to α-tubulin C-terminal tail (Howes et al., 2014; Panoutsopoulou et al., 2013; Stitziel et al., 2011), where TUBA4A mutations are clustered, may be responsible for this effect. Together, these results further suggest that missense mutants of TUBA4A weaken the microtubule network by a dominant-negative mechanism.

DISCUSSION

To summarize, we have used an unbiased case-control exome sequencing study to identify a statistically significant and replicable excess of rare damaging *TUBA4A*

variants in FALS. Disease-associated variants affect strongly conserved residues and in most cases are absent in over 13,000 controls. The positive identification of samples with mutations in the *SOD1* and *VCP* genes, as well as in the newly discovered ALS gene *MATR3* within the initial cohort, further proves the validity of our approach. Though our approach demonstrates the importance of a specific class of *TUBA4A* variant, an important limitation of the burden approach, which compares the number of rare variants in cases versus controls, is that it is not informative as to the effects of individual variants. It may therefore prove that not all reported patient mutations are pathogenically relevant or act with equal penetrance. An example of this is the identified K430N alteration that did not segregate in an affected first cousin suggesting that this is either a neutral variant or the two patients are phenocopies. However, our results from biological characterization provided strong evidence to support a deleterious effect of most variants. Specifically it was demonstrated that FALS associated variants 1) inefficiently form alpha/beta tubulin dimers *in vitro*; 2) display decreased incorporation into microtubules in cultured cells and 3) inhibit microtubule network assembly and reduce structural stability. Based on our functional data, TUBA4A mutants appear to disrupt microtubule dynamics and stability through a dominant-negative mechanism. Interestingly, the truncation mutant protein TUBA4A^{W407X} is deficient in forming dimers or incorporating into the microtubule network suggesting that it may have a decreased ability to act as a dominant negative. This is illustrated by our observation that in cells expressing the W407X mutant without aggregates, there is no obvious defect in the rate of microtubule polymerization after nocodazole treatment. However, since TUBA4A^{W407X} shows aggregation propensities analogous to other mutant proteins implicated in ALS

and other neurodegenerative diseases, its deleterious effect may be through a different mechanism, such as trapping tubulin-binding proteins into the aggregates or by over-burdening the ubiquitin proteasome system. Additionally, the mutant protein TUBA4A^{G43V}, found in a sporadic ALS case and in a control individual, did not display significant differences from the wild-type protein in its integration into microtubules nor in its influence on acetylation. These results suggest that this mutation may be a neutral variant or display lower penetrance.

Mutations in at least 7 other tubulin family members (TUBA1A (Keays et al., 2007; Kumar et al., 2010; Poirier et al., 2007), TUBA8 (Abdollahi et al., 2009), TUBB2B (Jaglin et al., 2009), TUBB3 (Poirier et al., 2010; Tischfield et al., 2010), TUBB5 (Breuss et al., 2012), TUBB4A (Hersheson et al., 2012; Tian et al., 2007), TUBG1 (Poirier et al., 2013)) have been previously described to cause several neurodevelopmental and neurodegenerative disorders, suggesting that mutations in different tubulin subunits may have specific effects within the central nervous system. For instance, mutations in the β-tubulin gene *TUBB3* have been shown to disrupt KIF-mediated axonal transport, resulting in widespread axon loss both in the CNS and in the peripheral nervous system (Niwa et al., 2013) while mutations in TUBA1A impairs neuronal migration, thus causing severe brain dysgenesis. Moreover, the progressive motor neuronopathy (*pmn*) mutant mouse, a commonly used model for human motor neuron disease, is the result of a mutation in the *Tubulin-specific Chaperone E* (*TBCE*) gene (Bömmel et al., 2002; Martin et al., 2002). Most mutant tubulin protein show similar functional defects compared to TUBA4A mutants, such as impaired dimerization and microtubule incorporation, and yet cause very different phenotypes. Interestingly, results from the BrainSpan Atlas show

that in the primary motor cortex, most α- and β-tubulin subunits responsible for developmental defects are highly expressed early during brain development and decrease with age, whereas *TUBA4A* levels increase dramatically (>50-fold) with age (Figure S13). These results are recapitulated in microarray data of developing mouse brain tissue (E14-P14)(Figure S14)(Pramparo et al., 2011) which show a ~30-fold increase of TUBA4A. Furthermore, similar to *TUBA4A*, expression of *TUBB4A* also increases over time (Figure S13-S14) and mutations in this gene are responsible for a disease with a onset age of 15-37 years (torsion dystonia type 4)(Hersheson et al., 2012). These observations may partially explain the difference between the neurodevelopmental and late onset symptoms associated to the different tubulin mutations.

TUBA4A is ubiquitously expressed in human tissues with its highest expression in brain (ArrayExpress, Accession E-MTAB-513 [Illumina BodyMap])(Rustici et al., 2013). Although a downregulation of genes encoding for α-tubulin subunits has been reported in spinal motor neurons of SALS patients (Jiang et al., 2005), no specific role has been described for TUBA4A in motor neurons so far. It must be noticed, however, that although the majority of known ALS-causing genes are ubiquitously expressed, very little is still known about their specific effects on motor neurons. TUBA4A joins other ALS-associated genes encoding for cytoskeletal proteins, such as PFN1 (Wu et al., 2012), DCTN1 (Puls et al., 2003), PRPH (Gros-Louis, 2004), and NEFH (Al-Chalabi et al., 1999), thus strengthening the hypothesis that alterations affecting the cytoskeleton architecture and dynamics have a major role in ALS pathogenesis.

SUPPLEMENTAL INFORMATION

Supplemental Information includes Supplemental Data (sixteen figures, and ten tables), Supplemental Experimental Procedures, Supplemental Text, Supplemental References and Supplemental Files (two Excel spreadsheets) and can be found with this article online.

ACKNOWLEDGMENTS

Funding was provided by the National Institutes of Health (NIH)/National Institute of Neurological Disorders and Stroke (NINDS) (R01NS065847 and R01NS073873 (JEL)), the American ALS Association (NT, VS, CES, JEL), the MND Association (NT, VS, CES, JEL), a Francesco Caleffi donation (NT, VS), the Medical Research Council, the Heaton-Ellis Trust and AriSLA co-financed with support of '5x1000'—Healthcare research of the Italian Ministry of Health (grants EXOMEFALS 2009 and NOVALS 2012 (NT, CG, VS, JEL)), the European Community's Seventh Framework Programme (FP7/2007-2013) under grant agreement number 259867, the National Institute for Health Research (NIHR) Dementia Biomedical Research Unit at South London (CES, AAC), Maudsley NHS Foundation Trust (CES, AAC), King's College London (CES, AAC), the Motor Neurone Disease Research Institute of Australia (Leadership Grant to IPB and a Bill Gole fellowship to KLW), the National Health and Medical Research Council of Australia (1004670), the Netherlands ALS Foundation and Project MinE. The views expressed are those of the authors and not necessarily those of the funding agencies. The authors thank Maryangel Jeon for excellent technical support and J.M.B.V de Jong for identification and selection of the Dutch FALS kindreds.

REFERENCES

Abdollahi, M.R., Morrison, E., Sirey, T., Molnár, Z., Hayward, B.E., Carr, I.M., Springell, K., Woods, C.G., Ahmed, M., Hattingh, L., et al. (2009). Mutation of the Variant α-Tubulin TUBA8 Results in Polymicrogyria with Optic Nerve Hypoplasia. The American Journal of Human Genetics *85*, 737–744.

Al-Chalabi, A., Andersen, P.M., Nilsson, P., Chioza, B., Andersson, J.L., Russ, C., Shaw, C.E., Powell, J.F., and Leigh, P.N. (1999). Deletions of the heavy neurofilament subunit tail in amyotrophic lateral sclerosis. Human Molecular Genetics *8*, 157–164.

Bömmel, H., Xie, G., Rossoll, W., Wiese, S., Jablonka, S., Boehm, T., and Sendtner, M. (2002). Missense mutation in the tubulin-specific chaperone E (Tbce) gene in the mouse mutant progressive motor neuronopathy, a model of human motoneuron disease. The Journal of Cell Biology *159*, 563–569.

Breuss, M., Heng, J.I.-T., Poirier, K., Tian, G., Jaglin, X.H., Qu, Z., Braun, A., Gstrein, T., Ngo, L., Haas, M., et al. (2012). Mutations in the β-Tubulin Gene TUBB5 Cause Microcephaly with Structural Brain Abnormalities. Cell Reports *2*, 1554–1562.

Chio, A., Calvo, A., Mazzini, L., Cantello, R., Mora, G., Moglia, C., Corrado, L., D'Alfonso, S., Majounie, E., Renton, A., et al. (2012). Extensive genetics of ALS: a population-based study in Italy. Neurology *79*, 1983–1989.

Cleveland, D.W., Kirschner, M.W., and Cowan, N.J. (1978). Isolation of separate mRNAs for alpha- and beta-tubulin and characterization of the corresponding in vitro translation products. Cell *15*, 1021–1031.

Gilissen, C., Hoischen, A., Brunner, H.G., and Veltman, J.A. (2011). Unlocking Mendelian disease using exome sequencing. Genome Biol *12*, 228.

Gros-Louis, F. (2004). A Frameshift Deletion in Peripherin Gene Associated with Amyotrophic Lateral Sclerosis. Journal of Biological Chemistry *279*, 45951–45956.

Hersheson, J., Mencacci, N.E., Davis, M., MacDonald, N., Trabzuni, D., Ryten, M., Pittman, A., Paudel, R., Kara, E., Fawcett, K., et al. (2012). Mutations in the autoregulatory domain of β-tubulin 4a cause hereditary dystonia. Ann. Neurol. *73*, 546–553.

Howes, S.C., Alushin, G.M., Shida, T., Nachury, M.V., and Nogales, E. (2014). Effects of tubulin acetylation and tubulin acetyltransferase binding on microtubule structure. Molecular Biology of the Cell *25*, 257–266.

Jaglin, X.H., Poirier, K., Saillour, Y., Buhler, E., Tian, G., Bahi-Buisson, N., Fallet-Bianco, C., Phan-Dinh-Tuy, F., Kong, X.P., Bomont, P., et al. (2009). Mutations in the β-tubulin gene TUBB2B result in asymmetrical polymicrogyria. Nat. Genet. *41*, 746–752.

Jiang, Y.-M., Yamamoto, M., Kobayashi, Y., Yoshihara, T., Liang, Y., Terao, S.,

Takeuchi, H., Ishigaki, S., Katsuno, M., Adachi, H., et al. (2005). Gene expression profile of spinal motor neurons in sporadic amyotrophic lateral sclerosis. Ann. Neurol. *57*, 236–251.

Johnson, J.O., Pioro, E.P., Boehringer, A., Chia, R., Feit, H., Renton, A.E., Pliner, H.A., Abramzon, Y., Marangi, G., Winborn, B.J., et al. (2014). Mutations in the Matrin 3 gene cause familial amyotrophic lateral sclerosis. Nat Neurosci *17*, 664–666.

Keays, D.A., Tian, G., Poirier, K., Huang, G.-J., Siebold, C., Cleak, J., Oliver, P.L., Fray, M., Harvey, R.J., Molnár, Z., et al. (2007). Mutations in alpha-tubulin cause abnormal neuronal migration in mice and lissencephaly in humans. Cell *128*, 45–57.

Kenna, K.P., McLaughlin, R.L., Byrne, S., Elamin, M., Heverin, M., Kenny, E.M., Cormican, P., Morris, D.W., Donaghy, C.G., Bradley, D.G., et al. (2013). Delineating the genetic heterogeneity of ALS using targeted high-throughput sequencing. J. Med. Genet. *50*, 776–783.

Kiezun, A., Garimella, K., Do, R., Stitziel, N.O., Neale, B.M., McLaren, P.J., Gupta, N., Sklar, P., Sullivan, P.F., Moran, J.L., et al. (2012). Exome sequencing and the genetic basis of complex traits. Nat. Genet. *44*, 623–630.

Kumar, R.A., Pilz, D.T., Babatz, T.D., Cushion, T.D., Harvey, K., Topf, M., Yates, L., Robb, S., Uyanik, G., Mancini, G.M.S., et al. (2010). TUBA1A mutations cause wide spectrum lissencephaly (smooth brain) and suggest that multiple neuronal migration pathways converge on alpha tubulins. Human Molecular Genetics *19*, 2817–2827.

Liu, J.S., Schubert, C.R., Fu, X., Fourniol, F.J., Jaiswal, J.K., Houdusse, A., Stultz, C.M., Moores, C.A., and Walsh, C.A. (2012). Molecular basis for specific regulation of neuronal kinesin-3 motors by doublecortin family proteins. Mol. Cell *47*, 707–721.

Martin, N., Jaubert, J., Gounon, P., Salido, E., Haase, G., Szatanik, M., and Guénet, J.-L. (2002). A missense mutation in Tbce causes progressive motor neuronopathy in mice. Nat. Genet. *32*, 443–447.

Matsuyama, A., Shimazu, T., Sumida, Y., Saito, A., Yoshimatsu, Y., Seigneurin-Berny, D., Osada, H., Komatsu, Y., Nishino, N., Khochbin, S., et al. (2002). In vivo destabilization of dynamic microtubules by HDAC6-mediated deacetylation. Embo J *21*, 6820–6831.

Niwa, S., Takahashi, H., and Hirokawa, N. (2013). β-Tubulin mutations that cause severe neuropathies disrupt axonal transport. Embo J *32*, 1352–1364.

Panoutsopoulou, K., Tachmazidou, I., and Zeggini, E. (2013). In search of low-frequency and rare variants affecting complex traits. Human Molecular Genetics *22*, R16–R21.

Piperno, G., LeDizet, M., and Chang, X.J. (1987). Microtubules containing acetylated alpha-tubulin in mammalian cells in culture. The Journal of Cell Biology *104*, 289–302.

Poirier, K., Keays, D.A., Francis, F., Saillour, Y., Bahi, N., Manouvrier, S., Fallet-Bianco, C., Pasquier, L., Toutain, A., Tuy, F.P.D., et al. (2007). Large spectrum of lissencephaly and pachygyria phenotypes resulting from de novo missense mutations in tubulin alpha 1A (TUBA1A). Hum. Mutat. *28*, 1055–1064.

Poirier, K., Lebrun, N., Broix, L., Tian, G., Saillour, Y., Boscheron, C., Parrini, E., Valence, S., Pierre, B.S., Oger, M., et al. (2013). Mutations in TUBG1, DYNC1H1, KIF5C and KIF2A cause malformations of cortical development and microcephaly. Nat. Genet. *45*, 639–647.

Poirier, K., Saillour, Y., Bahi-Buisson, N., Jaglin, X.H., Fallet-Bianco, C., Nabbout, R., Castelnau-Ptakhine, L., Roubertie, A., Attie-Bitach, T., Desguerre, I., et al. (2010). Mutations in the neuronal ß-tubulin subunit TUBB3 result in malformation of cortical development and neuronal migration defects. Human Molecular Genetics *19*, 4462–4473.

Pramparo, T., Libiger, O., Jain, S., Li, H., Youn, Y.H., Hirotsune, S., Schork, N.J., and Wynshaw-Boris, A. (2011). Global developmental gene expression and pathway analysis of normal brain development and mouse models of human neuronal migration defects. PLoS Genet. *7*, e1001331.

Puls, I., Jonnakuty, C., LaMonte, B.H., Holzbaur, E.L.F., Tokito, M., Mann, E., Floeter, M.K., Bidus, K., Drayna, D., Oh, S.J., et al. (2003). Mutant dynactin in motor neuron disease. Nat. Genet. *33*, 455–456.

Rustici, G., Kolesnikov, N., Brandizi, M., Burdett, T., Dylag, M., Emam, I., Farne, A., Hastings, E., Ison, J., Keays, M., et al. (2013). ArrayExpress update--trends in database growth and links to data analysis tools. Nucleic Acids Research *41*, D987–D990.

Stitziel, N.O., Kiezun, A., and Sunyaev, S. (2011). Computational and statistical approaches to analyzing variants identified by exome sequencing. Genome Biol *12*, 227.

Tennessen, J.A., Bigham, A.W., O'Connor, T.D., Fu, W., Kenny, E.E., Gravel, S., McGee, S., Do, R., Liu, X., Jun, G., et al. (2012). Evolution and Functional Impact of Rare Coding Variation from Deep Sequencing of Human Exomes. Science *337*, 64–69.

Tian, G., Kong, X.P., Jaglin, X.H., Chelly, J., Keays, D., and Cowan, N.J. (2007). A Pachygyria-causing -Tubulin Mutation Results in Inefficient Cycling with CCT and a Deficient Interaction with TBCB. Molecular Biology of the Cell *19*, 1152–1161.

Tian, G., Jaglin, X.H., Keays, D.A., Francis, F., Chelly, J., and Cowan, N.J. (2010). Disease-associated mutations in TUBA1A result in a spectrum of defects in the tubulin folding and heterodimer assembly pathway. Human Molecular Genetics *19*, 3599–3613.

Tischfield, M.A., Baris, H.N., Wu, C., Rudolph, G., Van Maldergem, L., He, W., Chan, W.-M., Andrews, C., Demer, J.L., Robertson, R.L., et al. (2010). Human TUBB3 mutations perturb microtubule dynamics, kinesin interactions, and axon guidance. Cell

140, 74–87.

Wu, C.-H., Fallini, C., Ticozzi, N., Keagle, P.J., Sapp, P.C., Piotrowska, K., Lowe, P., Koppers, M., McKenna-Yasek, D., Baron, D.M., et al. (2012). Mutations in the profilin 1 gene cause familial amyotrophic lateral sclerosis. Nature *488*, 499–503.

FIGURE LEGENDS

Figure 1. Rare variant analysis identifies TUBA4A mutations in FALS. (A) Manhattan plot displaying permutation-based corrected *P* values generated by a rare variant analysis of FALS are shown. The dotted line represents a $P_{corrected}$=0.05. The points in yellow, red and black for *TUBA4A* denote the *P*-value for the discovery, replication and joint analyses respectively. **(B)** The evolutionary conservation of TUBA4A mutations are displayed. Mutated residues are shown in red. **(C)** The interactions of bovine TUBA1B and TUBB2B with the rat kinesin KIF5B (Protein Data Bank accession 4ATX) are shown using the PyMOL Molecular Graphics System (v.1.5.0.5). All relevant residues are identical between bovine TUBA1B and human TUBA4A. Light blue: α-tubulin; green: β-tubulin; orange: kinesin; red: residues identified as mutants in this study or deleted in the W407X individual; spheres: residues involved in inter-protein interactions. As shown, the C-terminal region interacts with both the β -tubulin subunit and the kinesin motor domain.

Figure 2. Mutant TUBA4A alters microtubule polymerization. (A) Primary motor neurons transfected with HA-tagged TUBA4A constructs. **(B)** HEK293 cells transfected with wild-type or W407X mutant HA-TUBA4A constructs were immunostained for ubiquitin. Ubiquitin-positive aggregates were visible only in the HA-TUBA4A^{W407X}-transfected cells. **(C)** Non-denaturing (top) and SDS-gel electrophoresis (bottom) of HA-

TUBA4A constructs after *in vitro* translation. **(D)** The intensity of the bands representing the α/β tubulin dimers was quantified from 6 independent experiments. Bars represent mean and SEM (one-way ANOVA and Dunnett's *post hoc* test, * $p<0.05$, *** $p<0.001$). **(E)** Primary astroglial cells were transfected with the HA-TUBA4A constructs and fixed 4 days after transfection. The ratio between HA-TUBA4A protein distributions in filaments versus its overall levels was measured and divided into 4 categories from mainly filamentous to mainly diffuse. **(F)** The frequency of each phenotype was quantified and compared between the wild-type and mutant proteins (Kolmogorov-Smirnov test; n=75-90 cells per condition from 3 independent experiments, ** $p<0.01$, *** $p<0.001$). From left to right, bars represent the relative frequency of the normal, mild, moderate, and severe phenotypes. Red, HA; green, ubiquitin; blue, DAPI. White boxes indicate the regions enlarged in the insets. Scale bars: 10μm.

Figure 3. Mutant TUBA4A alters microtubule dynamics. (A, C) COS7 expressing wild-type and mutant TUBA4A were treated with 10μM nocodazole for 2 hours and allowed to recover in nocodazole-free medium for 2.5, 5, 10, or 15 minutes prior to fixation. Representative images are shown. Red, HA; green, TUBA4A; blue, DAPI. White boxes indicate the regions enlarged in the insets. Scale bars: 10μm. **(B, D)** The percentage of cells containing microtubules positive for the HA-tagged (red) or the endogenous TUBA4A protein (green) at different time points was quantified from more than 100 cells per condition from three independent experiments and compared between wild-type and mutant TUBA4A (one-way ANOVA and Dunnett's *post hoc* test;

n=3, * p<0.05, ** p<0.01, *** p<0.001). For the TUBA4A^{W407X} mutant, cells were analyzed separately based on the presence of cytoplasmic inclusions.

Figure 4. Mutant TUBA4A destabilizes the microtubule network. (A) PMNs transfected with wild-type or mutant TUBA4A constructs were permeabilzed with 0.1% Triton X-100 for 5 minutes prior to fixation. **(B, C)** The fluorescence intensity of HA-TUBA4A (red) and β-tubulin (green) was quantified and compared. Bars represent mean and SEM (Kruskas-Wallis test, n=23-34 cells per condition from 3 independent experiments, * p<0.05, ** p<0.01, *** p<0.001). **(D, E)** Acetylated tubulin (green) levels were measured in motor neurons expressing TUBA4A mutants (red). Representative images are shown. Bars represent mean and SEM (one way ANOVA and Dunnett's *post hoc* test, n=30-45 cells per condition from 3 independent experiments, * p<0.05, ** p<0.01). DAPI (blue) was used to identify the nucleus. Scale bars: 10μm.

Figure 1

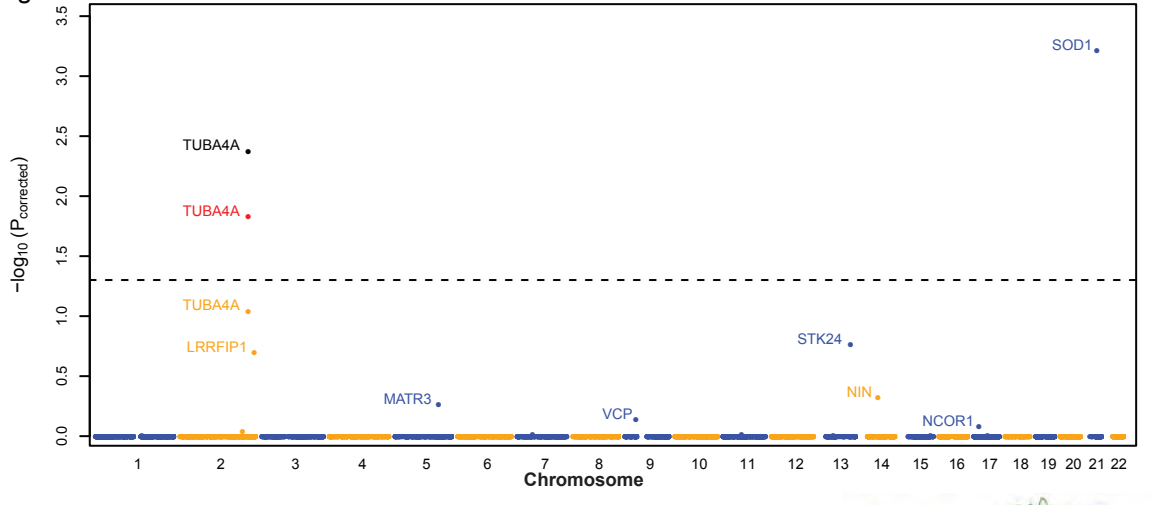

B

Mutation	G43V	T145P	R215C	R320C/H	A383T	W407X	K430N
	-----V-----	-----P-----	-----C-----	-----C----- -----H-----	-----T-----	-----X-----	-----N-----
Human	SDKTIGGGDDS	SFGGGTGSGFT	YDICRRNLDIE	CCLLYRGDVVP	LSNTTAIAEAW	RAFVHWYVGEG	VEEYDKELAAM
Chimp	SDKTIGGGDDS	SFGGGTGSGFT	YDICRRNLDIE	CCLLYRGDVVP	LSNTTAIAEAW	RAFVHWYVGEG	VEEYDKELAAM
Rhesus	SDKTIGGGDDS	SFGGGTGSGFT	YDICRRNLDIE	CCLLYRGDVVP	LSNTTAIAEAW	RAFVHWYVGEG	VEEYDKELAAM
Mouse	SDKTIGGGDDS	SFGGGTGSGFT	YDICRRNLDIE	CCLLYRGDVVP	LSNTTAIAEAW	RAFVHWYVGEG	VEEYDKELAAM
Rat	SDKTIGGGDDS	SFGGGTGSGFT	YDICRRNLDIE	CCLLYRGDVVP	LSNTTAIAEAW	RAFVHWYVGEG	VEEYDKELAAM
Rabbit	SDKTIGGGDDS	SFGGGTGSGFT	YDICRRNLDIE	CCLLYRGDVVP	LSNTTAIAEAW	RAFVHWYVGEG	VEEYDKELAAM
Cow	SDKTIGGGDDS	SFGGGTGSGFT	YDICRRNLDIE	CCLLYRGDVVP	LSNTTAIAEAW	RAFVHWYVGEG	VEEYDKELAAM
Dog	SDKTIGGGDDS	SFGGGTGSGFT	YDICRRNLDIE	CCLLYRGDVVP	LSNTTAIAEAW	RAFVHWYVGEG	VEEYDKELAAM
Elephant	SDKTIGGGDDS	SFGGGTGSGFT	YDICRRNLDIE	CCLLYRGDVVP	LSNTTAIAEAW	RAFVHWYVGEG	VEEYDKELAAM
Zebrafish	SDKTIGGGDDS	SFGGGTGSGFT	YDICRRNLDIE	CCLLYRGDVVP	LSNTTAIAEAW	RAFVHWYVGEG	VEEYDKELAAM

C

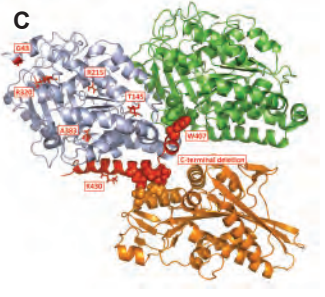

Figure 2

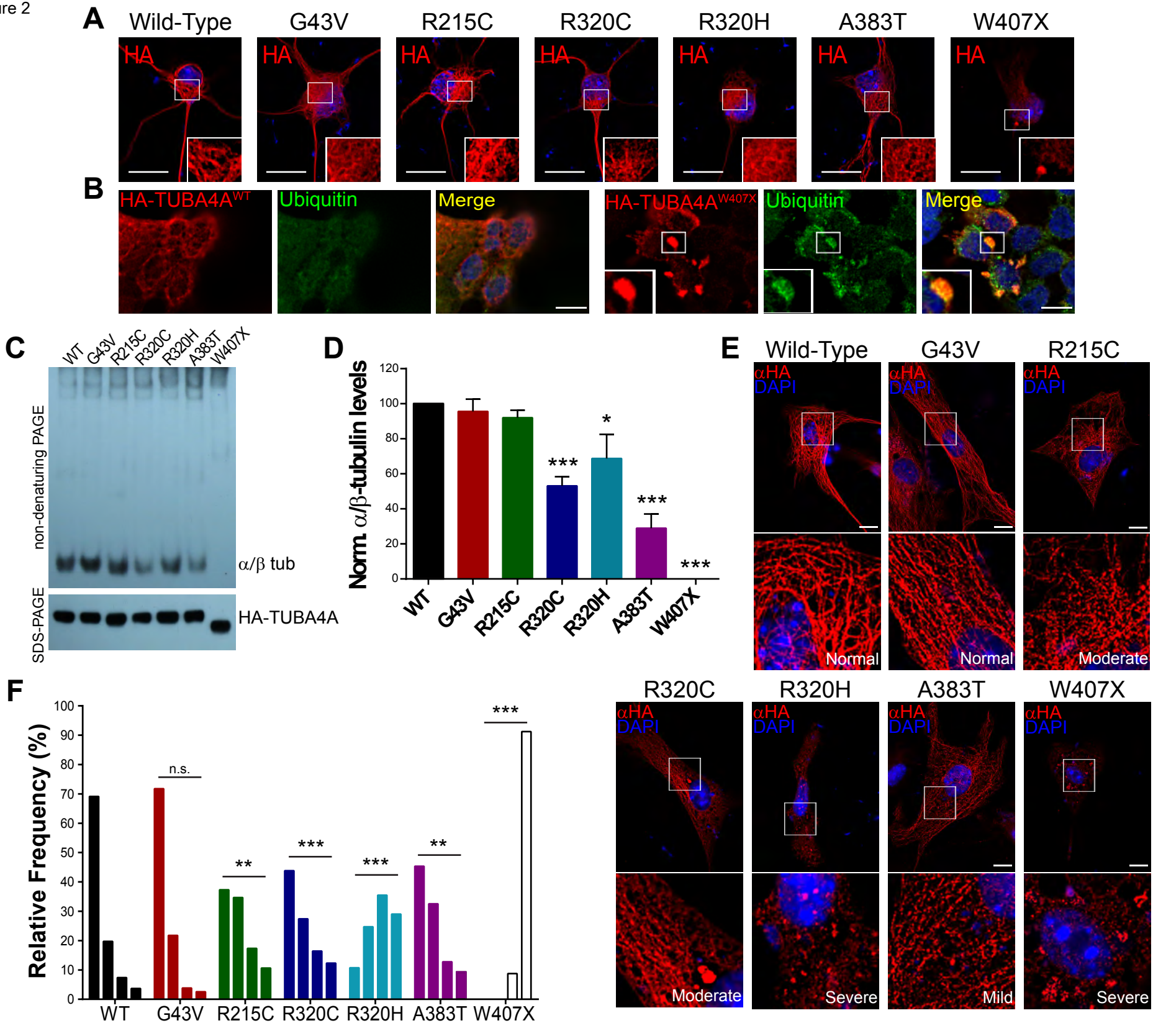
A
Wild-Type
G43V
R215C
R320C
R320H
A383T
W407X
HA
B
HA-TUBA4A^WT
Ubiquitin
Merge
HA-TUBA4A^W407X
C
WT
G43V
R215C
R320C
R320H
A383T
W407X
non-denaturing PAGE
α/β tub
SDS-PAGE
HA-TUBA4A
D
Norm. α/β-tubulin levels
120
100
80
60
40
20
0
*
***
***
***
WT
G43V
R215C
R320C
R320H
A383T
W407X
E
Wild-Type
G43V
R215C
αHA
DAPI
Normal
Normal
Moderate
F
Relative Frequency (%)
100
90
80
70
60
50
40
30
20
10
0
n.s.
**
***
***
**
***
WT
G43V
R215C
R320C
R320H
A383T
W407X
R320C
R320H
A383T
W407X
αHA
DAPI
Moderate
Severe
Mild
Severe

Figure 3

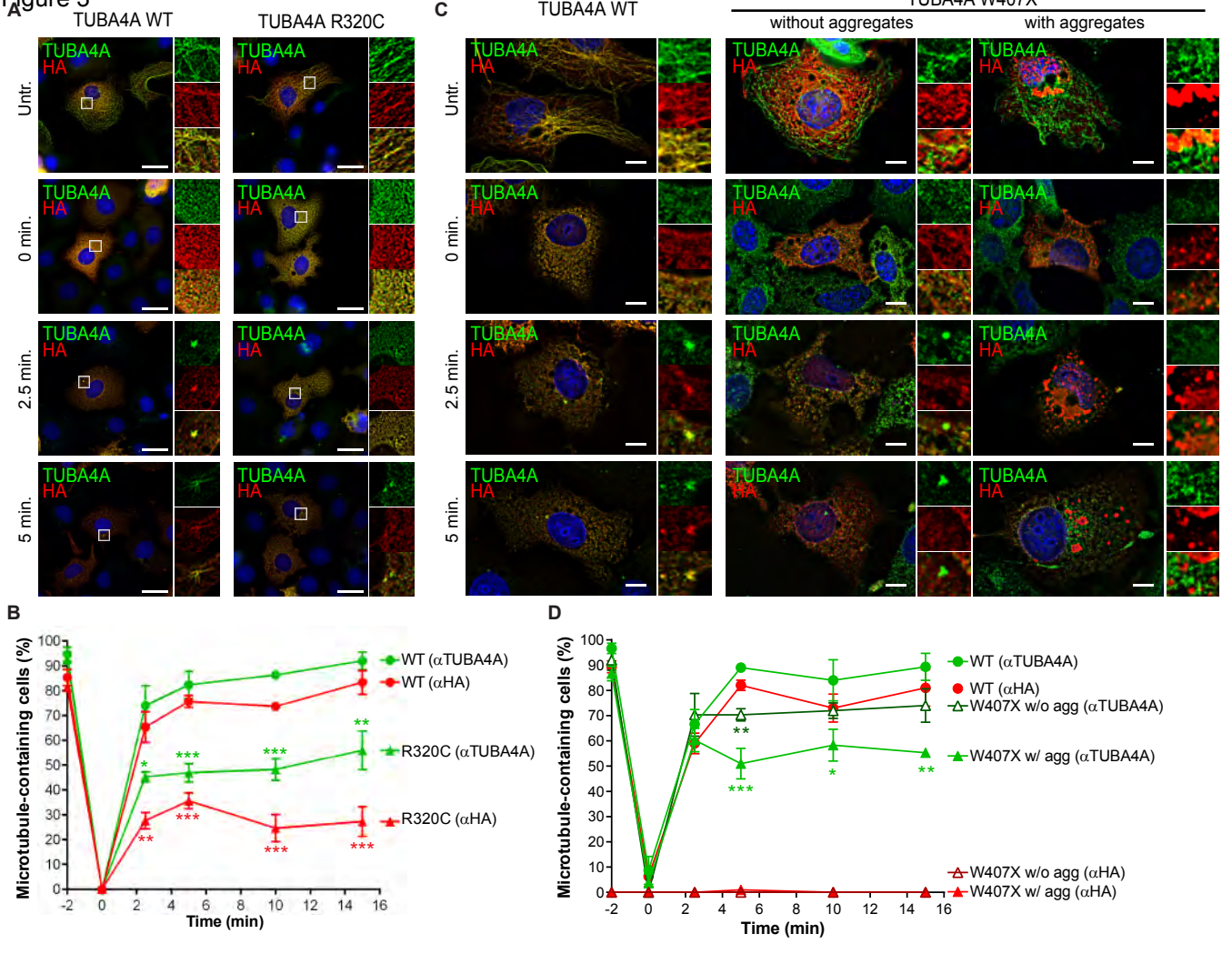
A
TUBA4A WT
TUBA4A R320C
C
TUBA4A WT
TUBA4A W407X
without aggregates
with aggregates
Untr.
0 min.
2.5 min.
5 min.
TUBA4A
HA
B
Microtubule-containing cells (%)
Time (min)
WT (αTUBA4A)
WT (αHA)
R320C (αTUBA4A)
R320C (αHA)
D
Microtubule-containing cells (%)
Time (min)
WT (αTUBA4A)
WT (αHA)
W407X w/o agg (αTUBA4A)
W407X w/ agg (αTUBA4A)
W407X w/o agg (αHA)
W407X w/ agg (αHA)

Figure 4

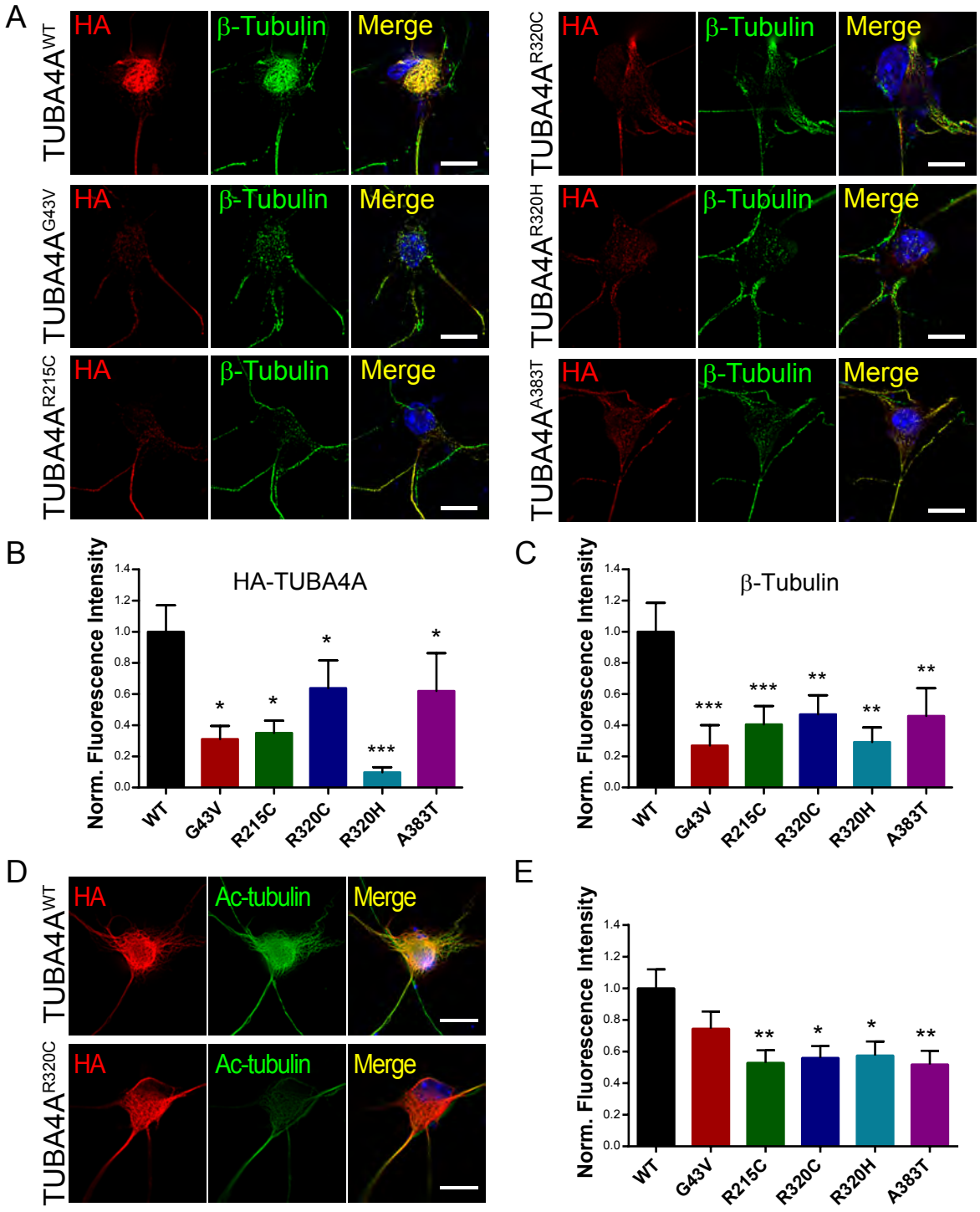
A
TUBA4A^WT
TUBA4A^G43V
TUBA4A^R215C
TUBA4A^R320C
TUBA4A^R320H
TUBA4A^A383T
HA
β-Tubulin
Merge
B
HA-TUBA4A
Norm. Fluorescence Intensity
C
β-Tubulin
WT
G43V
R215C
R320C
R320H
A383T
D
Ac-tubulin
E

INVENTORY OF SUPPLEMENTAL INFORMATION

Figure S1. Manhattan plot of uncorrected *P*-values obtained by gene-based rare-variant analysis. Represents data shown in Figure 1A prior to multiple test correction.

Figure S2. Sequencing quality of TUBA4A by the NHLBI's Exome Variant Server. Provides addition support that the top hit in Figure 1A is not due to poor sequencing.

Figure S3. QQ Plots of rare variant analysis for familial ALS. Demonstrates the results shown in Figure 1A do not display genomic inflation.

Figure S4. Chromatograms of TUBA4A mutations. Provides sequence confirmation of the mutations identified in TUBA4A from the analysis in Figure 1A.

Figure S5. Familial ALS pedigrees with TUBA4A mutations. Provides the family structure of individuals harboring TUBA4A mutations identified from the analysis in Figure 1A and subsequent replication set.

Figure S6. Protein fractionation of TUBA4A mutants. Provides confirmation of the aggregation observed in Figure 2B.

Figure S7. Solubility of TUBA4A mutants. Provides confirmation of the aggregation observed in Figure 2B.

Figure S8. TUBA4A staining of SALS cases and controls. Demonstrates a lack of aggregation, as opposed to the mutant W407X in Figure 2B, with wild-type TUBA4A in sporadic ALS.

Figure S9. Lack of co-localization of wild-type TUBA4A with TDP-43 aggregates. Demonstrates a lack of aggregation, as opposed to the mutant W407X in Figure 2B, with wild-type TUBA4A and mutant TDP-43 co-expressed in cells.

Figure S10. Quantitation of incorporation of TUBA4A in the microtubule network. Provides additional detail of the results presented in Figure 2E and F.

Figure S11. Mutant R320C TUBA4A alters microtubule dynamics. Provides supporting results for Figure 3A and B.

Figure S12. Altered microtubule acetylation in mutant TUBA4A expressing cells. Figures for additional mutants shown in Figure 4D.

Figure S13. Relative expression of tubulin subunits in the primary motor cortex with age. Provides support for material presented in the Discussion.

Figure S14. Relative expression of tubulin subunits during mouse brain development. Provides support for material presented in the Discussion.

Figure S15. Relative expression of exogenous TUBA4A. Represents level of exogenous expression of TUBA4A in assays presented in Figures 2-4.

Figure S16. Stratification analysis of exome sequenced samples. Provides analysis for the case samples used in Figure 1A.

Table S1. Summary of samples subject to exome sequencing in the discovery cohort. Provides information on the cases used in Figure 1A.

Table S2. Summary statistics for exome sequencing of the FALS discovery set. Provides information on the exome sequencing results used in Figure 1A.

Table S3. Coding variants identified by exome sequencing. Provides information on the exome sequencing results used in Figure 1A.

Table S4. Ranking and *P* values of top hits from the gene-based rare variant analysis. Provides the top hits for the data presented in Figure 1A as well as additional rare variant testing.

Table S5. Description of mutations identified in TUBA4A. Provides detailed information of the mutations identified in the discover analysis and replication analysis (Figure 1B).

Table S6. Description of non-synonymous variants identified in FALS and in EVS European Americans. Provides detailed information of the TUBA4A variants present in the cases and controls used to generate Figure 1A.

Table S7. Summary of samples screened for *TUBA4A* mutations in the replication cohort. Country breakdown of the samples used in the replication set described in the main text.

Table S8. Summary of ALS samples with known mutations/expansions sequenced for *TUBA4A* mutations. Breakdown of number of samples with known ALS mutations as described in the main text.

Table S9. Clinical characteristics of ALS patients with TUBA4A mutations. Provides additional information on the samples with TUBA4A mutation identified from the discovery analysis and replication set (Figure 1B).

Table S10. Analysis of TUBA4A mutations in control populations. Detailed information on TUBA4A mutation identified from the discovery analysis and replication set (Figure 1B).

Supplemental Spreadsheet: BurdenTestResults.xls. Provides burden test results for all genes and all filtering methods including PolyPhen-2 (Figure 1A).

Supplemental Spreadsheet: TopGeneVariants.xls. Provides all variants in the top 10 genes used for the burden test for all filtering methods including PolyPhen-2 (Figure 1A).

SUPPLEMENTAL DATA

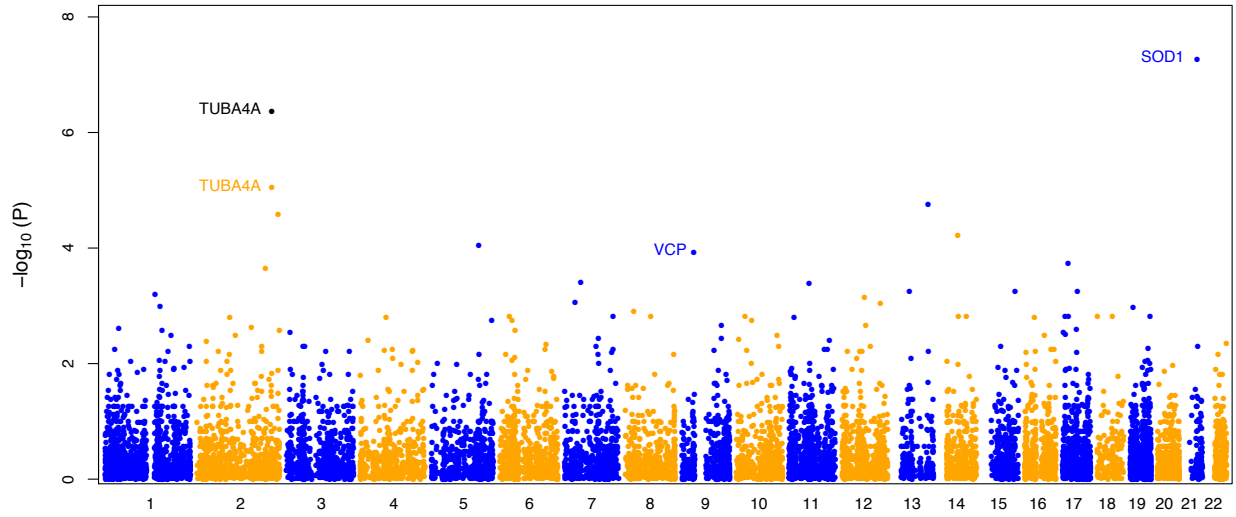

Figure S1. Manhattan plot of uncorrected *P*-values obtained by gene-based rare-variant analysis. Gene-based rare variant analysis was perform using variants either predicted to be damaging using PolyPhen-2 or resulting in a stop gain/loss. Variants were also only considered if they exhibited minor allele frequencies in keeping with previously reported ALS mutations. The point in black represents the *P*-value of *TUBA4A* after the incorporation of data generated from the replication set. A Manhattan plot using corrected *P*-values is shown in Figure 1A.

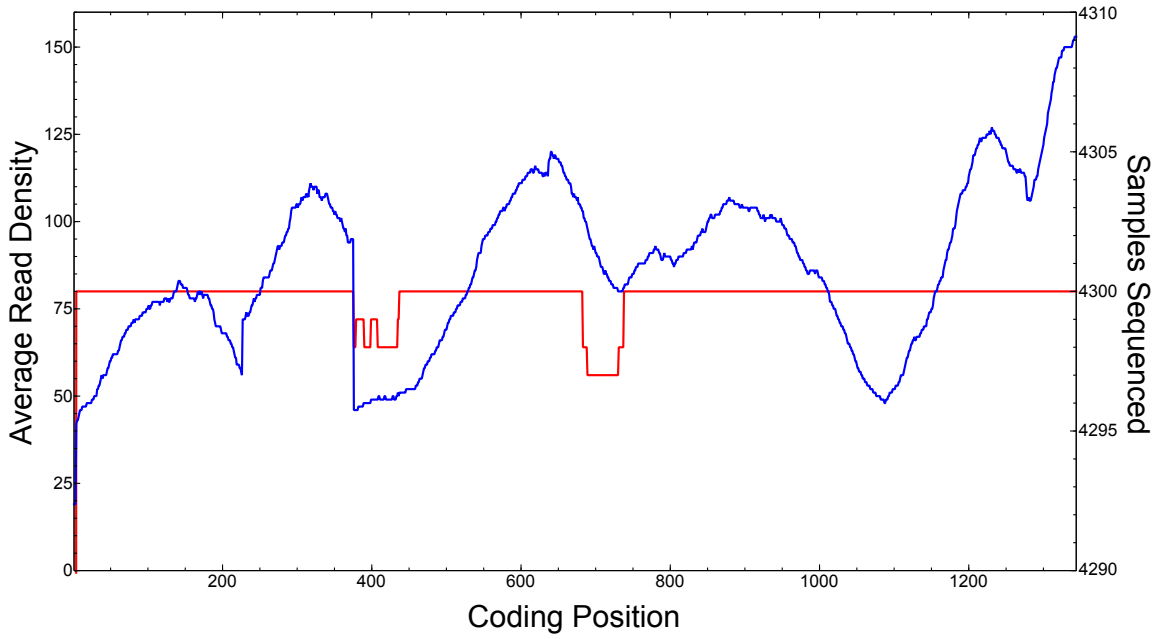

Figure S2. Sequencing quality of TUBA4A by the NHLBI's Exome Variant Server. The average read density of TUBA4A at each coding position by the ESP is plotted in blue. The number of samples that passed quality control measures, out of 4300 samples, at each position is plotted in red.

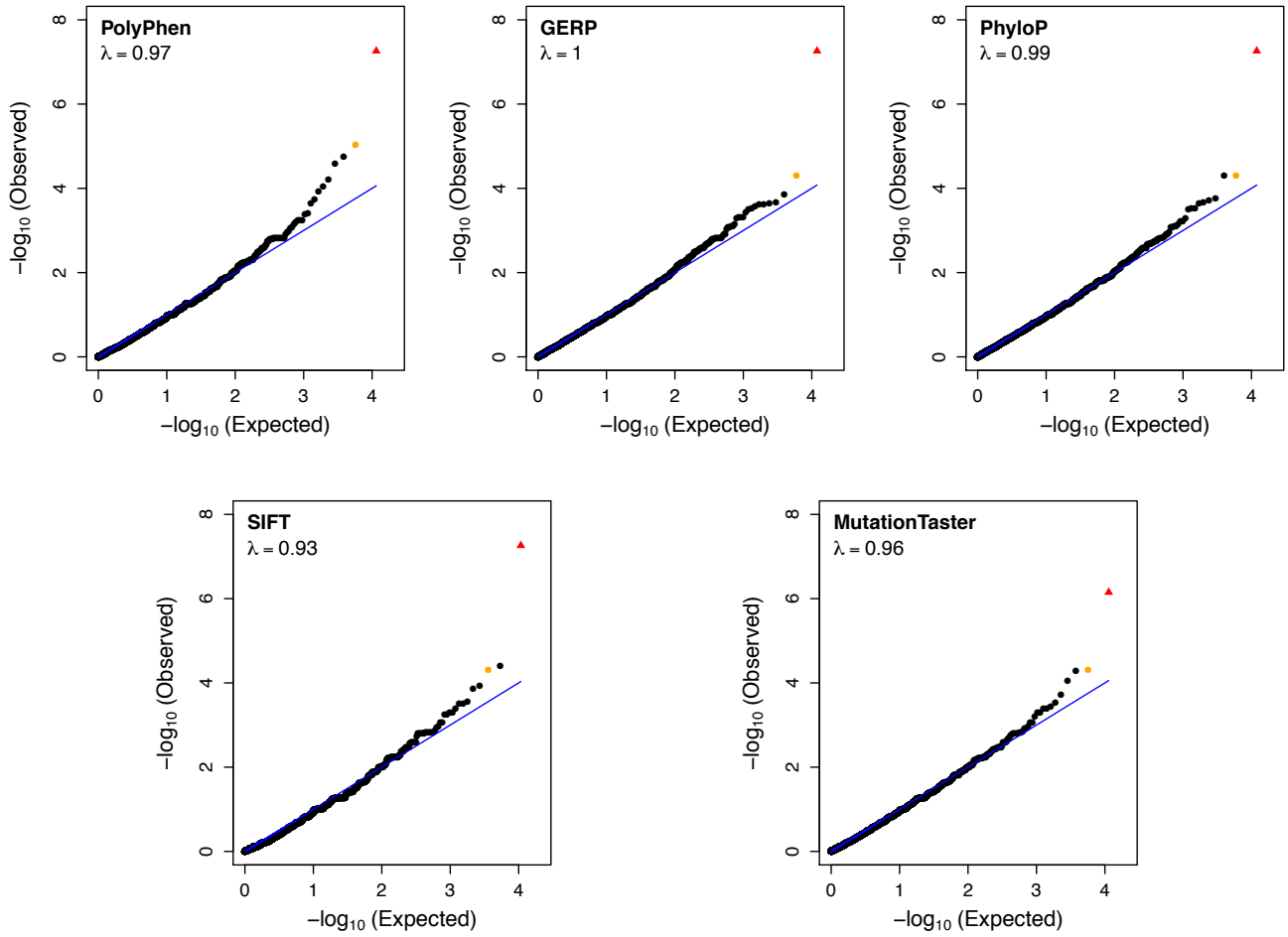

Figure S3. QQ Plots of rare variant analysis for familial ALS. Variants identified through exome sequencing were filtered based on the method displayed. The remaining variants were subject to rare variant analysis. Expected *P* values are plotted against those obtained through our analysis. The black line represents results that would be obtained under the null hypothesis. The red triangle represents the *P* value resulting from spiked SOD1 mutant samples and the orange point represents the *P* value for *TUBA4A*. The genomic inflation factor is shown.

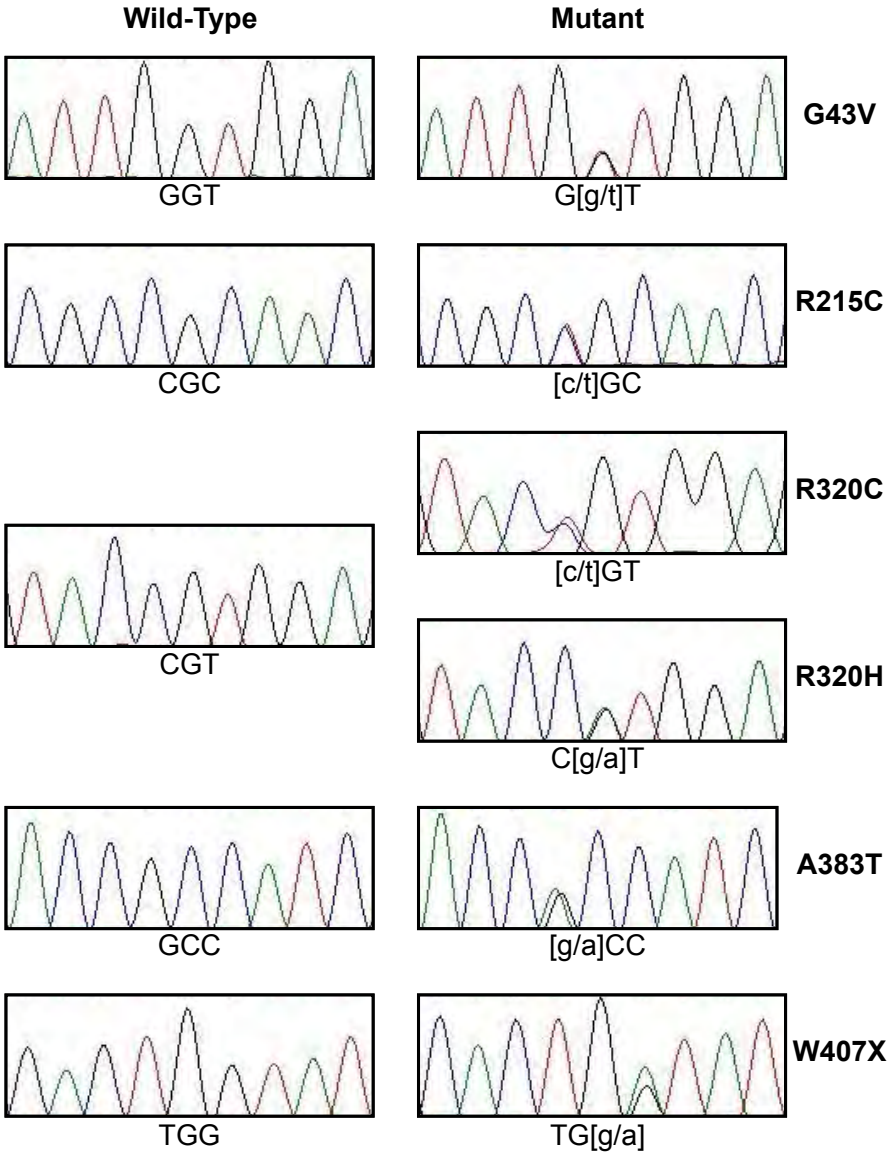

Figure S4. Chromatograms of TUBA4A mutations. Sequence traces of representative samples harboring either wild-type (left column) or mutant (right column)

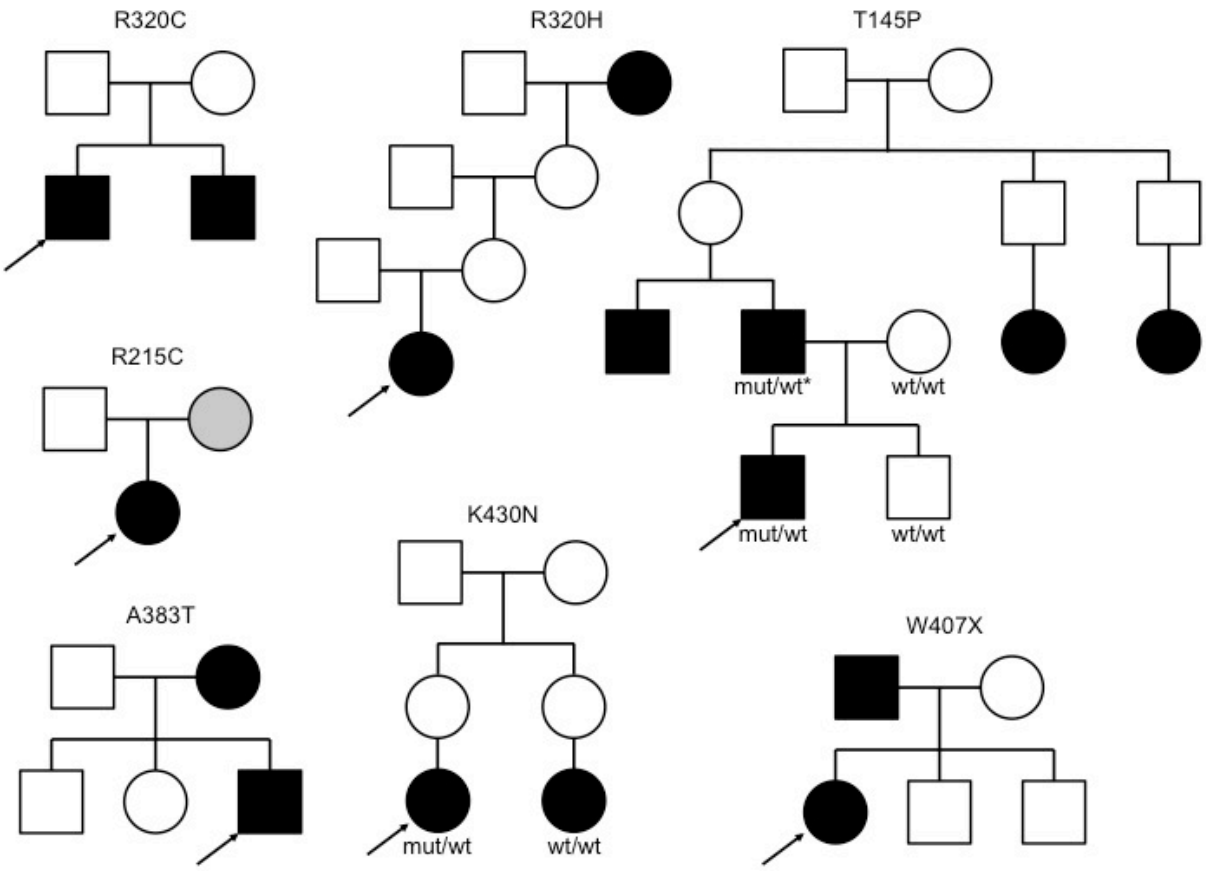

Figure S5. Familial ALS pedigrees with TUBA4A mutations. Family structure for each mutation is shown. Black: ALS; grey: frontotemporal dementia; white: unaffected. The proband is indicated with an arrow. The asterisk indicates the genotype was inferred from the other family members.

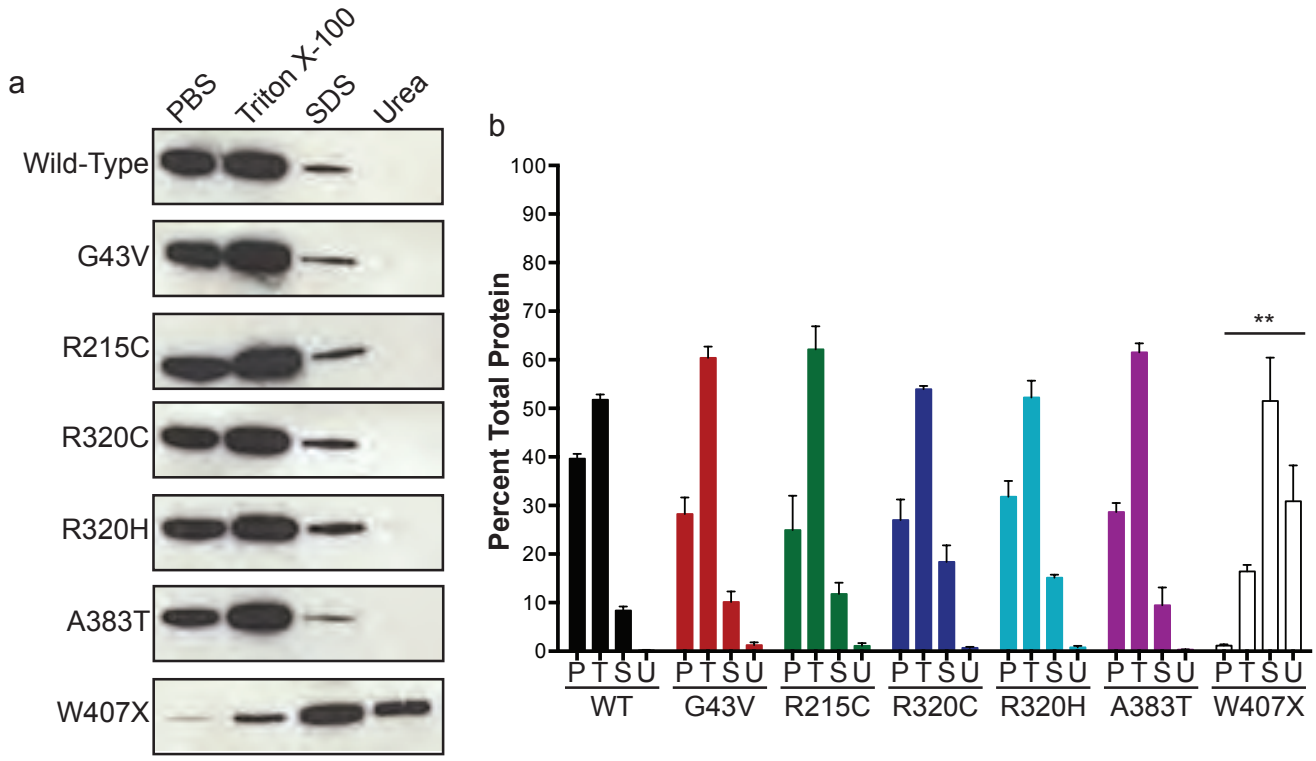

Figure S6. Protein fractionation of TUBA4A mutants. (A) HEK cells were transfected with constructs expressing wild-type and mutant TUBA4A. Cellular lysates were subject to sequential extractions using the buffers indicated and immunblotted with anti-HA antibody. As shown, the majority of W407X mutant protein is insoluble in Triton X-100 whereas the wild-type and missense mutants are soluble. **(B)** HA-TUBA4A levels were quantified in each fraction and represented as percentage of the total HA-TUBA4A protein. Bars represent mean and SEM (one-way ANOVA and Dunnett's *post hoc* test, n=3, ** $P<0.01$). P, PBS; T, Triton X-100; S, SDS; U, urea.

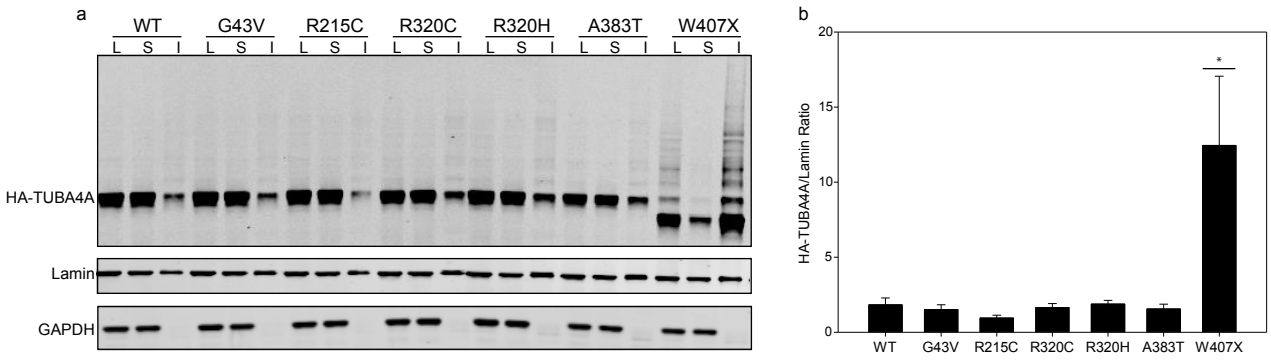

Figure S7. Solubility of TUBA4A mutants. (A) HEK cells were transfected with constructs expressing wild-type and mutant TUBA4A. Total lysate (L), soluble (S) and insoluble (I) fractions were subject to Western blotting using antibodies directed against HA, Lamin and GAPDH. **(B)** Expression levels were quantified and the ratio of HA signal in the insoluble fraction to Lamin signal was calculated. Bars represent the mean and SEM (one way Kruskal-Wallis ANOVA and Student-Newman-Keuls *post hoc* test, n=4, * $P<0.05$).

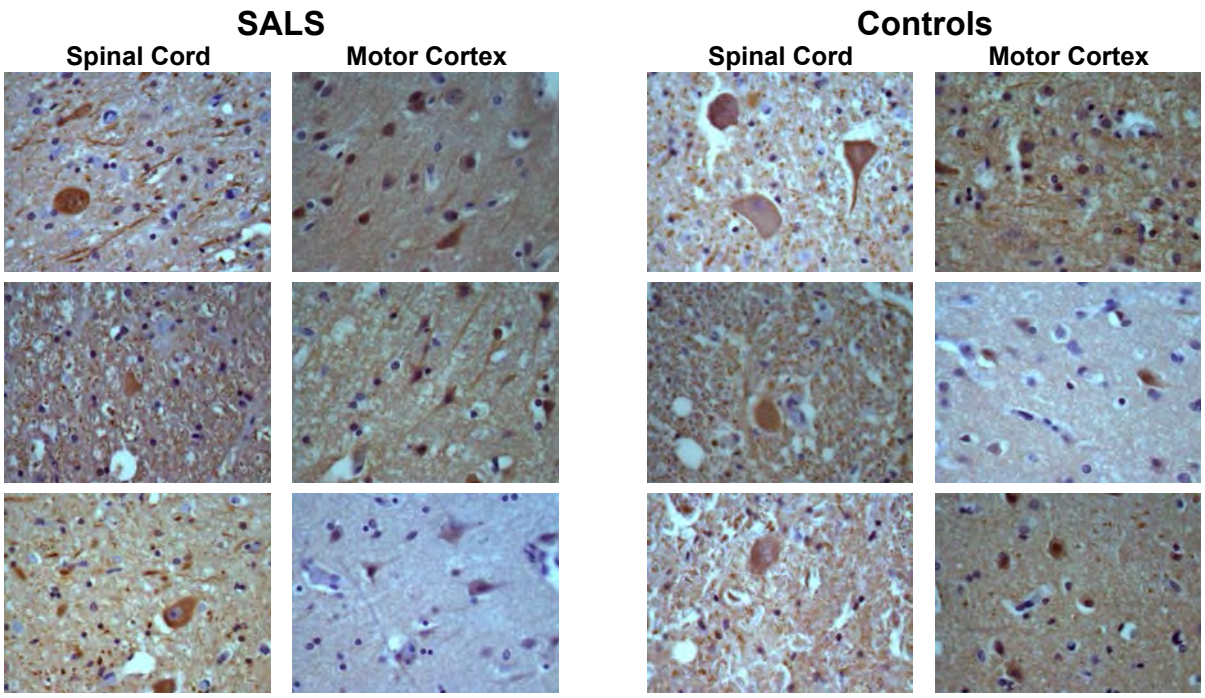

Figure S8. TUBA4A staining of SALS cases and controls. Sections of spinal cord and motor cortex from 3 different SALS cases and controls were stained with an antibody to TUBA4A that specifically targets the C-terminal part of the protein, which differs from other members of the alpha-tubulin family. SALS cases were positive for TDP-43 aggregates and negative for known causative mutations. As shown, immunohistochemistry did not detect aggregates of TUBA4A or differences between case and control samples. Clear staining of the perikarya and neuropil region in both the spinal cord and motor cortex was observed.

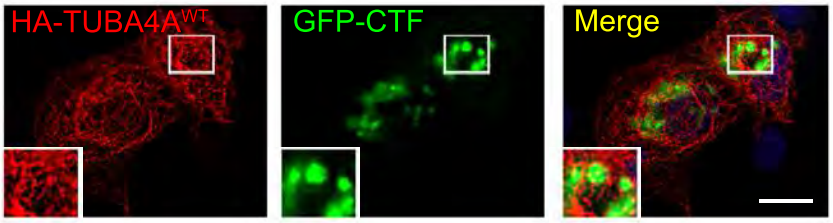

Figure S9. Lack of co-localization of wild-type TUBA4A with TDP-43 aggregates. COS7 cells were co-transfected with constructs expressing wild-type HA-TUBA4A and a GFP-labeled C-terminal fragment of TDP-43, which produces cellular aggregates. At twenty-four hours post transfection, the cells were fixed and stained with anti-HA antibodies. Scale: 10 μm.

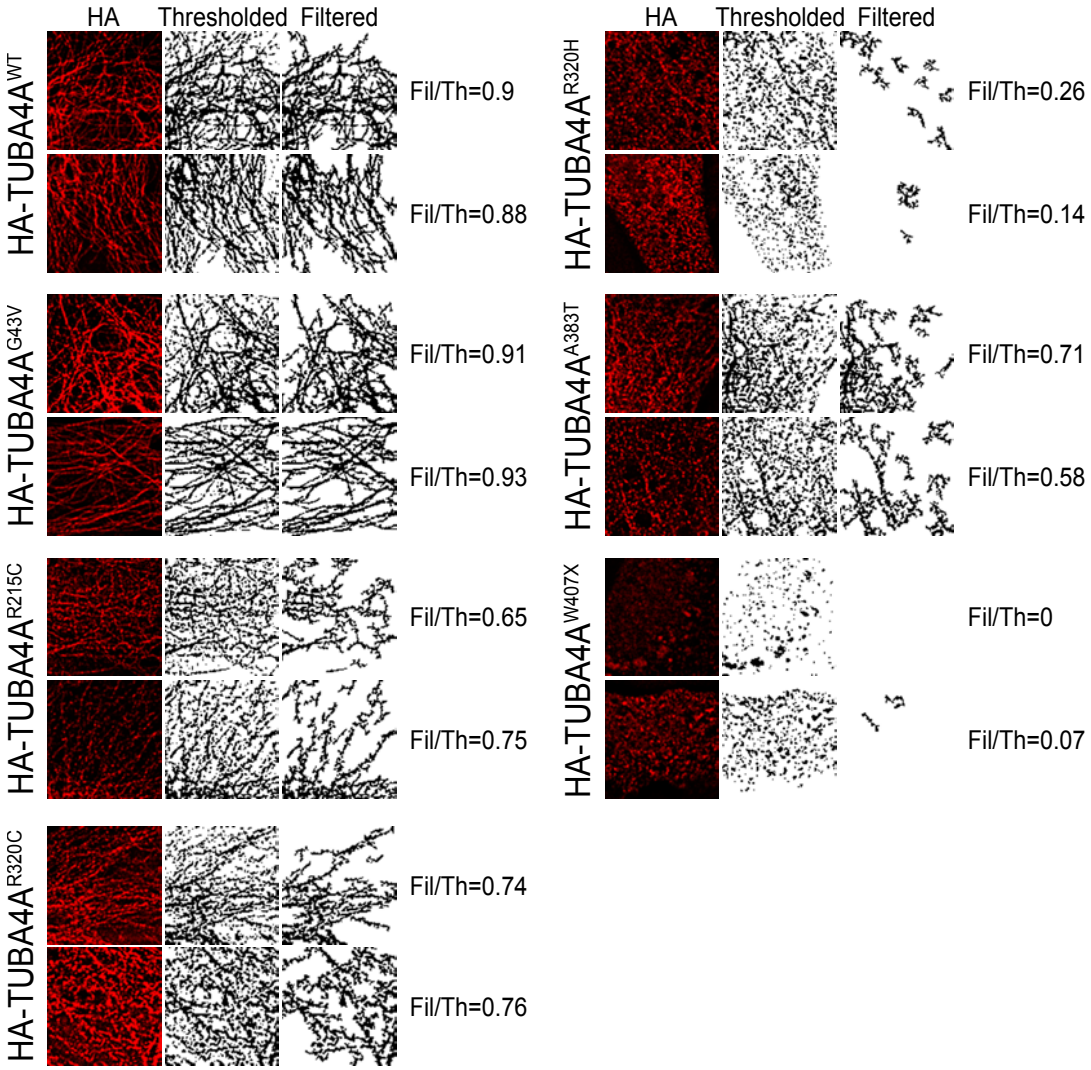

Figure S10. Quantitation of incorporation of TUBA4A in the microtubule network. Primary astroglial cells were transfected with the HA-TUBA4A constructs and fixed 4 days after transfection. After staining, the cytoskeletal incorporation of HA-tagged TUBA4A was quantitated as described in the Methods section. Briefly, ImageJ was used to apply a circularity filter to a thresholded image to remove granular staining. The resulting image represented the filamentous HA staining. The ratio between the fluorescence intensities of the filtered cytoskeleton versus the thresholded image resulted in an incorporation index ranging from 0 (no incorporation) to 1 (complete microtubule incorporation). Examples of the quantitation of images are shown.

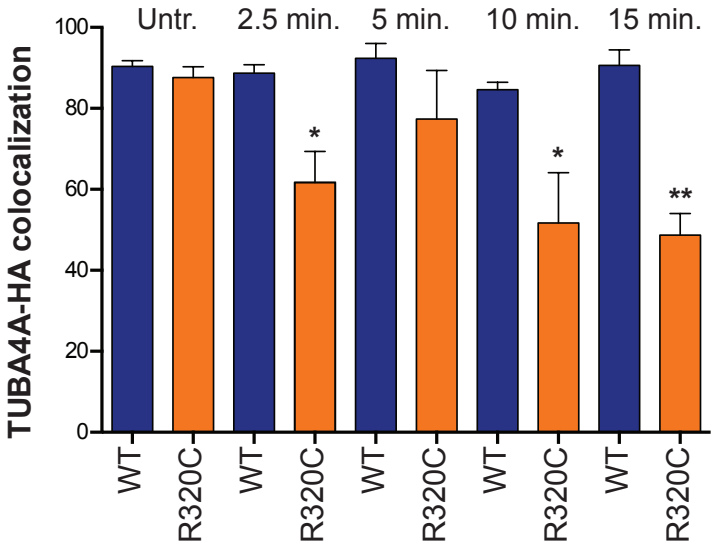

Figure S11. Mutant R320C TUBA4A alters microtubule dynamics. COS7 expressing wild-type and R320C TUBA4A were treated with nocodazole as described in Figure 3. The percentage of cells containing microtubules positive for both HA and TUBA4A protein is reduced in mutant TUBA4A-expressing cells compared to the wild-type control. Bars represent mean and SEM (Student's t test; n=3, * $p<0.05$, ** $p<0.01$).

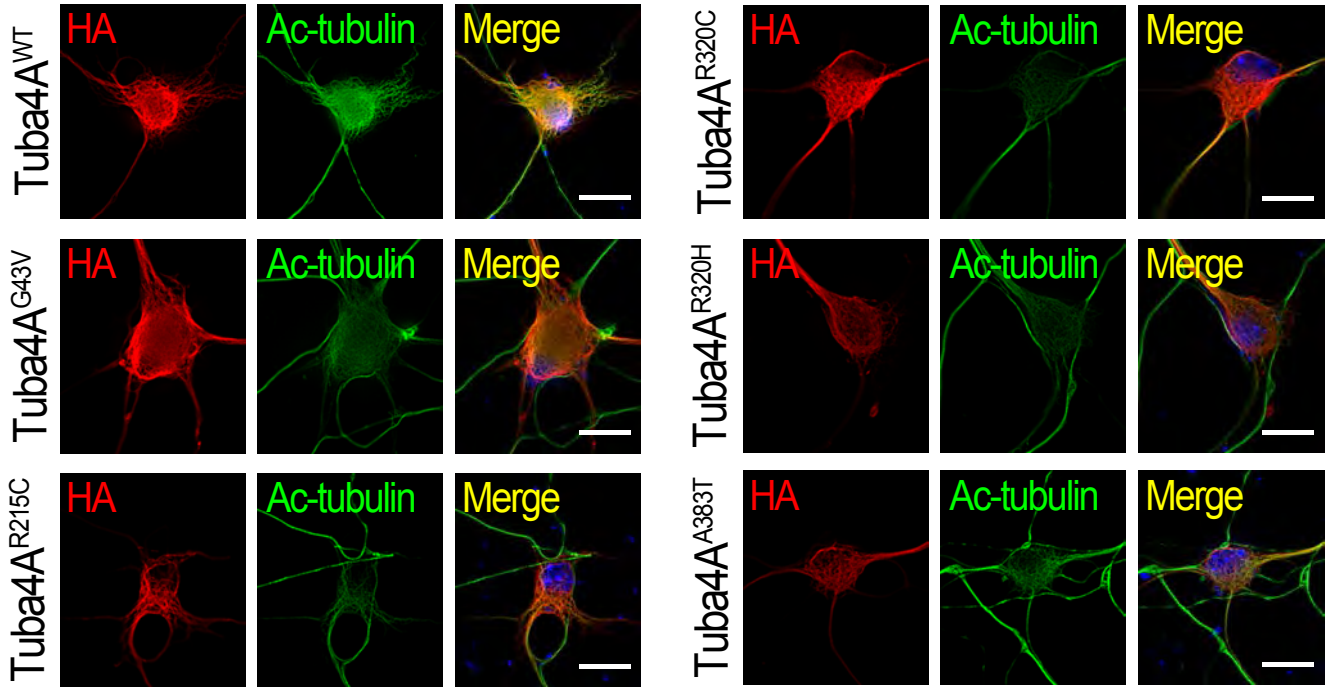

Figure S12. Altered microtubule acetylation in mutant TUBA4A expressing cells. Representative images of PMNs transfected with HA-tagged TUBA4A mutants (red) and immunostained with an antibody specific to acetylated tubulin (green). DAPI (blue) was used to identify the nucleus. Scale bars: 10 μm.

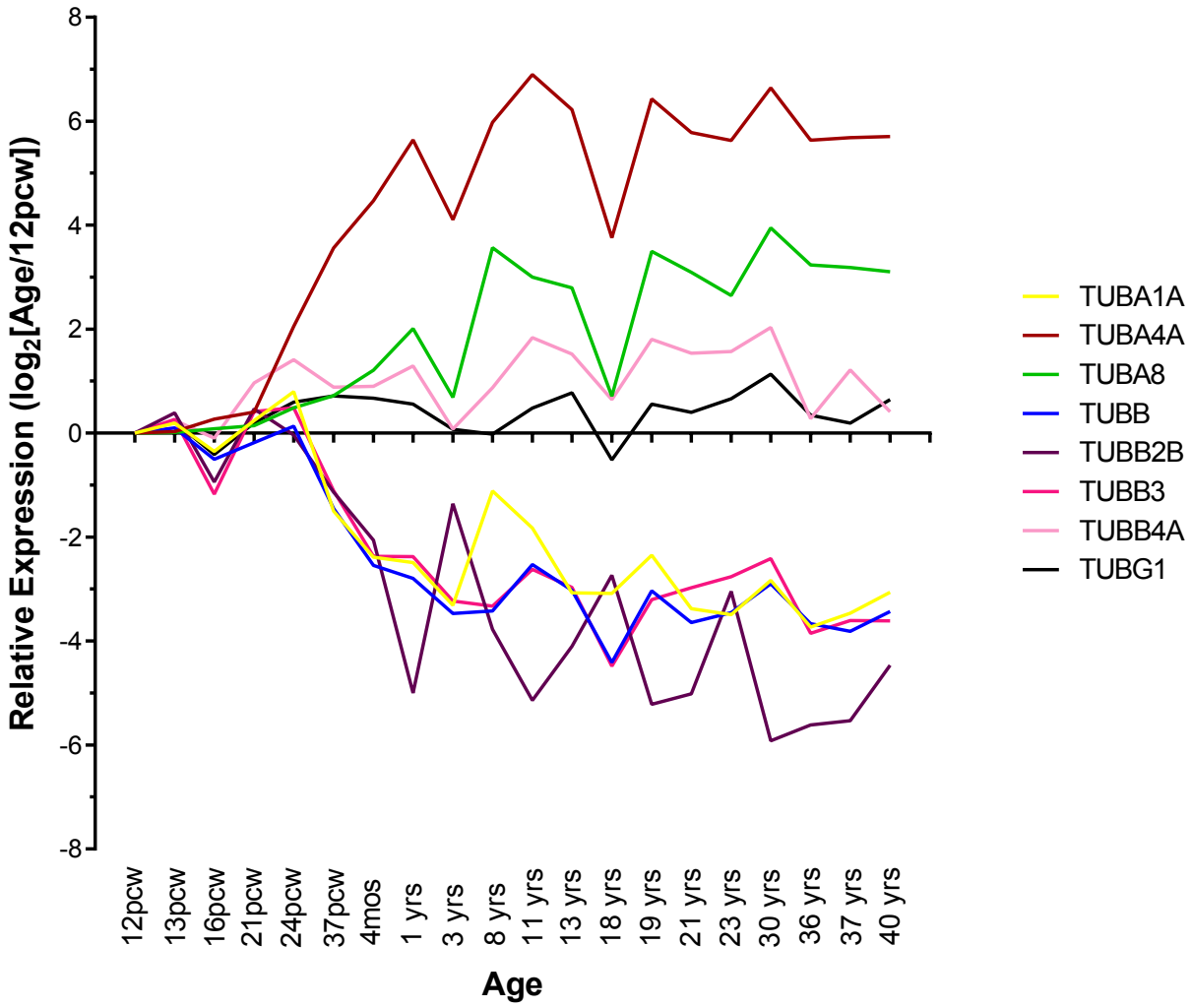

Figure S13. Relative expression of tubulin subunits in the primary motor cortex with age. RNA-Seq results derived from the primary motor cortex were downloaded from the BrainSpan Atlas of the Developing Human Brain (http://www.brainspan.org). Expression at each age was normalized to the expression at 12 pcw. For time points in which multiple samples were sequenced, the average was used. The relative expression (log_2) was plotted for each age. As shown, TUBA4A expression increases over time whereas most other subunits responsible for developmental defects display their highest expression prenatally.

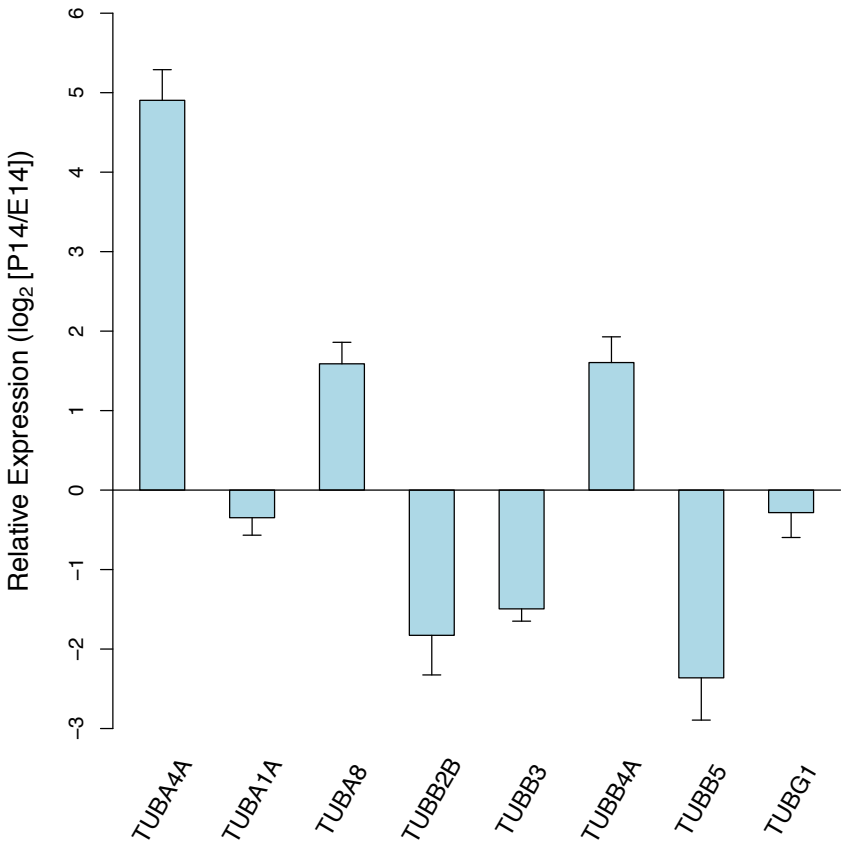

Figure S14. Relative expression of tubulin subunits during mouse brain development. Microarray expression data was downloaded from the NCBI's Gene Expression Omnibus (GEO)(DataSet Record GDS4502) for the tubulin subunits shown. Changes in expression in mouse brains (n=6) between embryonic day 14 and postpartum day 14 are plotted. Hybridizations were performed on the Affymetrix Mouse Genome 430 2.0 Array. Error bars represent standard deviations. Similar to results in human primary motor cortex, TUBA4A expression increases over time whereas most other subunits responsible for developmental defects display their highest expression prenatally.

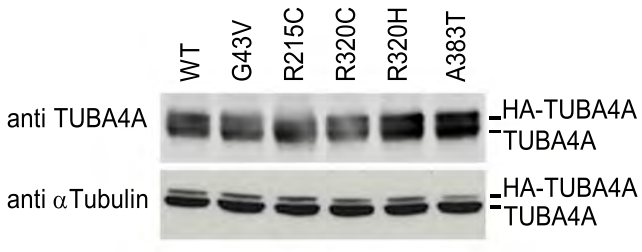

Figure S15. Relative expression of exogenous TUBA4A. HEK293 cells were transfected with HA-TUBA4A constructs and protein lysates collected 48 hours after transfection. The expression level of the HA-tagged proteins was compared to endogenous TUBA4A (*top panel*) or to overall α Tubulin expression (*bottom panel*) using specific antibodies (TUBA4A, Abgent; αTubulin, clone DM1A, Sigma Aldrich). All HA-TUBA4A proteins were expressed at similar levels, with an approximate 1:1 and 0.2:1 ratio compared to endogenous TUBA4A and all α Tubulins, respectively. The epitopes recognized by both antibodies are deleted in the TUBA4A^{W407X} mutant, which was thus not included in this analysis.

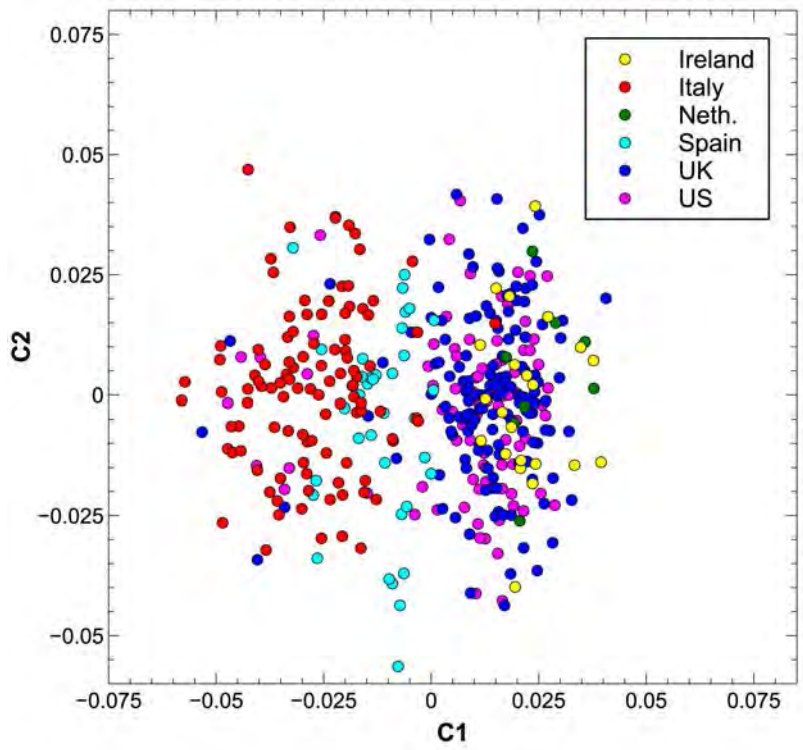

Figure S16. Stratification analysis of exome sequenced samples. Exome sequenced samples were subject to stratification analysis using the software application package PLINK. Pairwise genome-wide identity-by-state distances were calculated followed by linkage hierarchical cluster analysis and classical multidimensional scaling.

	FALS	Controls
Ireland	16	6
Italy	97	6
Netherlands	8	0
Spain	29	6
United Kingdom	132	7
United States	81	6
Total	363	31

Table S1. Summary of samples subject to exome sequencing in the discovery cohort.

Total Samples	403
Cases	372
Controls	31
Total reads	41,430,525,586
Average reads per sample	102,805,274
Total aligned reads	38,907,252,470
Average aligned reads per sample	96,544,051
Average % reads aligned	95.04%
Total aligned bases	3,229,103,417,870
Average aligned bases per sample	8,012,663,568
Total on target bases	1,301,439,397,693
Average on target bases per sample	3,229,378,158
Average mean target coverage per sample	90.44
Average % target bases with 2x coverage per sample	97.04%
Average % target bases with 10x coverage per sample	93.11%
Average % target bases with 20x coverage per sample	88.06%
Average % target bases with 30x coverage per sample	81.96%

Table S2. Summary statistics for exome sequencing of the FALS discovery set.

	Total	Average Per Sample
Coding SNPs	165,934	15935.69
Non-synonymous SNPs	99,910	7575.88
Synonymous SNPs	66,024	8359.81
Rare Coding SNPs (MAF<0.005)	111,394	1442.66
Rare Non-synonymous SNPs	70,878	790.64
Rare Synonymous SNPs	40,516	652.02
Novel Coding SNPs	41,431	118.87
Novel Non-synonymous SNPs	28,011	79.88
Novel Synonymous SNPs	13,420	38.98

Table S3. Coding variants identified by exome sequencing.

	PolyPhen-2		SIFT		MutationTaster		GERP		PhyloP	
Rank	Gene	*P*	Gene	*P*	Gene	*P*	Gene	*P*	Gene	*P*
1	TUBA4A	9.09E-06	SIDT2	3.84E-05	TUBA4A	4.87E-05	TUBA4A	4.87E-05	TUBA4A	4.87E-05
2	STK24	1.76E-05	TUBA4A	4.87E-05	SLAMF7	5.24E-05	PKD1L1	1.38E-04	PKD1L1	4.90E-05
3	LRRFIP1	2.61E-05	ALDH2	1.34E-04	ASNSD1	9.09E-05	ALDH2	2.20E-04	FARP1	1.69E-04
4	NIN	6.07E-05	NIN	2.82E-04	LRRFIP1	1.92E-04	JAZF1	2.26E-04	KCTD20	1.94E-04
5	MATR3	9.09E-05	PRICKLE1	3.15E-04	XYLT1	2.89E-04	FARP1	2.35E-04	ALDH2	2.20E-04
6	NCOR1	1.86E-04	GTF3C1	3.15E-04	NCOR1	3.57E-04	NCOR1	2.44E-04	JAZF1	2.26E-04
7	CLK1	2.26E-04	STK24	4.14E-04	MSLN	4.14E-04	KCTD20	2.74E-04	NCOR1	2.98E-04
8	PKD1L1	3.94E-04	MAPK13	4.91E-04	ING5	4.14E-04	XYLT1	2.98E-04	XYLT1	2.98E-04
9	OR10W1	4.14E-04	ATRN	4.91E-04	RASSF4	4.91E-04	GLYAT	3.14E-04	GLYAT	3.14E-04
10	C15orf32	5.58E-04	INPP1	5.58E-04	PPM1G	4.91E-04	BTBD16	3.72E-04	ASNSD1	5.17E-04

Table S4. Ranking and *P* values of top hits from the gene-based rare variant analysis.

Mutation	Chr:Position	Reference Allele	Alternative Allele	Codons	Exon	Country
G43V	2:220116828	C	A	GGT-GtT	2	Italy
T145P	2:220115988	T	G	ACT-cCT	4	US
R215C	2:220115778	G	A	CGC-tGC	4	Spain
R320C	2:220115463	G	A	CGT-tGT	4	Italy
R320H	2:220115462	C	T	CGT-CaT	4	UK
A383T	2:220115274	C	T	GCC-aCC	4	Italy
K430N	2:220115131	C	G	AAG-AAc	4	Netherlands
W407X	2:220115200	C	T	TGG-TGa	4	Italy

Table S5. Description of mutations identified in TUBA4A.

	Mutation	PolyPhen-2 Score	Prediction	Frequency
FALS	R215C	0.036	Benign	1/363
	R320H	0.822	Possibly Damaging	1/363
	R320C	0.917	Possibly Damaging	1/363
	A383T	0.995	Probably Damaging	1/363
	W407X	N/A	N/A	1/363
				Total: 5/363
European EVS	V68A	0.004	Benign	1/4300
	I276V	0	Benign	1/4300
	V375M	0.231	Benign	1/4300
				Total: 3/4300

Table S6. Description of non-synonymous variants identified in FALS and in EVS European Americans.

	FALS
Australia	63
Canada	52
Italy	4
Netherlands	37
Spain	10
United States	106
Total	272

Table S7. Summary of samples screened for *TUBA4A* mutations in the replication cohort.

	FALS
C9orf72	24
SOD1	32
TARDBP	13
FUS	12
PFN1	3
UBQLN2	3
VAPB	2
Total	89

Table S8. Summary of ALS samples with known mutations/expansions sequenced for *TUBA4A* mutations.

Mutation	Gender	ALS family history	Other ND family history	Age at onset (yrs.)	Site of onset	Disease Duration (mo.)	Clinical Phenotype	Dementia	Atypical features
G43V	M	SALS	dementia	52	spinal	45	UMN/LMN	yes (FTD)	no
T145P	M	FALS	dementia	48	spinal	69	UMN/LMN	no	no
R215C	F	FALS	dementia	78	spinal	n/a	UMN/LMN	yes (FTD)	no
R320C	M	FALS	no	64	spinal	12	UMN/LMN	no	no
R320H	F	FALS	no	41	spinal	33	UMN/LMN	no	no
A383T	M	FALS	no	71	spinal	18	UMN/LMN	no	no
K430N	F	FALS	no	64	spinal	42	UMN/LMN	no	no
W407X	F	FALS	no	66	spinal	36	UMN/LMN	no	no

Table S9. Clinical characteristics of ALS patients with TUBA4A mutations. Disease duration is calculated to the last follow-up. ND stands for other neurodegenerative disorders.

Mutation	EVS-European Americans	EVS-African Americans	1000Genomes Project	Internal Sequencing	Total
G43V	0/4300	0/2200	0/1053	1/5510	1/13,063
T145P	0/4300	0/2200	0/1053	0/5510	0/13,063
R215C	0/4300	0/2200	0/1053	0/5510	0/13,063
R320C	0/4300	0/2200	0/1053	0/5510	0/13,063
R320H	0/4300	0/2200	0/1053	0/5510	0/13,063
A383T	0/4300	1/2200	0/1053	0/5510	1/13,063
K430N	0/4300	0/2200	0/1053	0/5510	0/13,063
W407X	0/4300	0/2200	0/1053	0/5510	0/13,063

Table S10. Analysis of TUBA4A mutations in control populations.

SUPPLEMENTAL EXPERIMENTAL PROCEDURES

Human subjects and Plasmids.

DNA samples were collected from familial and sporadic ALS cases and control individuals after informed consent was obtained. All protocols were approved by the Institutional Review Boards at the institutions involved. A subset of the samples was obtained from the NINDS Repository at Coriell Cell Repositories. All FALS were screened for known causative mutations/repeat expansions in *SOD1*, *C9orf72*, *TARDBP*, *FUS*, *PFN1*, *UBQLN2*, *OPTN*, *VCP* and *ANG* and eliminated if a causative alteration was observed. Expression constructs were created by synthesizing the wild-type and mutant coding region with an HA epitope tag at the N-terminus (DNA2.0) and subcloning into the vector pJ603. HA-tagged TUBA4A constructs were initially tested in HEK293 cells. Similar expression to the endogenous protein was achieved after 48 hours in transiently transfected cells (Figure S15). The vector expressing the GFP-labeled C-terminal fragment of TDP-43 (amino acids 208-414) was described previously (Fallini et al., 2012).

Exome Sequencing and Rare Variant Analysis

Exome sequencing reads were aligned to a human reference (hg19) using BWA (Burrows-Wheeler Aligner) and processed using the Genome Analysis ToolKit (GATK). After removal of duplicate reads, indel realignment (GATK IndelRealigner), and base quality recalibration (GATK TableRecalibration) was performed. Variant detection and genotyping were performed using the UnifiedGenotyper (UG) tool from GATK. Variants not passing quality control criteria were eliminated (QD<5.0, HRun>3, MQ<40.0, FS>60.0, HaplotypeScore>13.0, MQRankSum< -12.5, ReadPosRankSum< -8.0) and genotypes with low quality (GQ<50) were set to missing. Samples were also excluded if they demonstrated low call rate (<0.75), relatedness to another sample (portion of the genome IBD > 0.2 or clinically reported), excess homozygosity/heterozygosity or if the gender determined by genotypes did not match the clinically reported gender. Stratification analysis was additionally applied to all remaining samples based on the distribution of pairwise genome-wide identity-by-state distances followed by complete linkage hierarchical cluster analysis and classical multidimensional scaling (Figure S16). Outlying samples were eliminated resulting in the final set of FALS used for rare variant analysis.

Rare variant analyses were performed by logistic regression of case-control status with respect to the aggregated count of minor alleles in a given gene window. Regression was performed using Firth's penalized likelihood method to avoid errors of model fitting in the event of data separation (where gene variants occur exclusively in the case or control cohort)(Heinze and Schemper, 2002). For controls, genotype summaries from 4300 European Americans were downloaded from the NHLBI's Exome Variant Server. These genotypes were randomly assigned to 4300 simulated individuals. Variants were filtered to those showing 90% call rate in either ESP data set or FALS. Gene selection was based on the initial set that passed quality control standards of the ESP study (14,931 autosomal genes). These genes were further restricted to those which displayed an 85% call rate over 85% of the coding region in the EVS resulting in the final set of 12,487 genes subject to rare variant analysis.

Variants were annotated as damaging by PolyPhen-2 (score> 0.446) or representing stop gain/loss variants. Additional filtering procedures included SIFT (“damaging”), Mutation Taster ("disease causing automatic" or “disease causing”), GERP (GERP++ score>0), and phyloP (score>0). Variants that did not display a 90% call rate in either cases or controls were eliminated from the analysis. Gene windows and predicted variant effects were defined based on protein coding RefSeq transcripts only. Variants were only included for analysis if the associated minor allele frequency did not exceed what would be expected of a typical ALS mutation on the basis of prior publications. Specifically, Mendelian ALS variants identified to date have generally been reported to account for <1% of population based patient cohorts (Chio et al., 2012; Kenna et al., 2013). The lifetime risk of ALS is ~1/400 (Johnston et al., 2006), meaning that even in the event of penetrance as low as 50%, it would not be expected to observe a given ALS mutation in more than a single control ($p<0.05$). To allow for the potential of a single control occurrence and up to 3 case occurrences (~1% of patients), a maximum minor allele frequency of 0.0004 (4 occurrences) was imposed. Multiple testing correction was performed through permutation correction as recommended by (Kiezun et al., 2012). Briefly, the significance of each gene association in the observed dataset was calculated. Case-control labels were then randomly shuffled 10,000 times and the logistic regression analysis was repeated on each permuted dataset to generate a null p-value distribution. For each gene p-value from the observed dataset analysis, $P_{corrected}$ was calculated as the proportion of permuted datasets where an association of equal or greater significance was observed across any gene. This corresponds to a direct and empirical measure of family-wise error rate which is preferable to Bonferroni correction for reasons discussed in (Kiezun et al., 2012). The genomic inflation factor was calculated as previously described (Dadd et al., 2009). All data processing and rare variant analyses were performed using scripts prepared for bash version 4.2.24, python version 2.6.5 and R version 3.0.1.

Motor neuron culture and transfection

Primary motor neurons were isolated from E12.5 mouse embryos as previously described (Liu et al., 2012; Oprea et al., 2008). Briefly, spinal cords were dissociated in 0.1% trypsin for 12 minutes at 37ºC, and motor neurons were isolated by density centrifugation on a 6% Optiprep (Sigma-Aldrich) cushion. Cells were plated on poly-ornithine and laminin-coated glass coverslips in growth medium (Neurobasal, 2% horse serum, 2% B27, 10nM BDNF, CNTF, GDNF) and transfected at 2 days *in vitro* (DIV) with Neuromag (OZ Bioscience) as previously described (Fallini et al., 2010). Motor neurons were fixed 4 days post transfection (dpt) with 4% paraformaldehyde for 15 minutes and processed for immunofluorescence. For the extraction of cytosoluble proteins, motor neurons were permeabilized at 7 dpt with 0.1% Triton-X100 in cytoskeletal stabilizing buffer (4M Glycerol, 25mM PIPES, 1mM EGTA, 1mM $MgCl_2$) for 5 minutes prior to fixation. After blocking in 5% bovine serum albumin (BSA) for 45 minutes, cells were hybridized with the primary antibodies (mouse anti-HA 1:1000, MMS-101R-200, Covance; rabbit anti-HA 1:100, Sigma-Aldrich; mouse anti-ubiquitin 1:100, Life Technologies; rabbit anti-β-tubulin 1:200, Cell Signaling Technology; mouse anti-acetylated tubulin 1:500, Sigma-Aldrich) diluted in 5% BSA for 1 hour at room temperature or overnight at 4ºC. AlexaFluor 488 and AlexaFluor 594-conjugated

secondary antibodies were diluted 1:500 in 5% BSA and hybridized for 1 hour at room temperature. Coverslips were mounted with Prolong Gold mounting medium Life Technologies) and imaged with a widefield fluorescence microscope equipped with a high resolution/sensitivity camera (Leica). Image stacks (10 stacks, 0.2µm thickness) were deconvolved (Autoquant, MediaCybernetics) and analyzed using ImageJ.

Tubulin Dimerization Assay

In vitro translation of HA-TUBA4A was performed using the TNT T7 Coupled Reticulocyte Lysate system (Promega). For non-denaturing gel electrophoresis, the products were diluted 1:1 in sample buffer (160 mM MES pH 6.86, 2mM $MgCl_2$, 2 mM EGTA, 1 mM GTP, 20% Glycerol), immediately loaded onto a non denaturing gel (4.5% polyacrylamide in 80mM MES pH 6.86, 1mM $MgCl_2$, 1mM EGTA, 1mM GTP) and run at 95 volts for 1.5 hours. For SDS-gel electrophoresis, the reaction products were diluted in 2X Laemmli buffer, boiled for 5 minutes and loaded onto a 4-20% Mini-PROTEAN TGX gel (Bio-Rad). Proteins were transferred to a 0.45 µm nitrocellulose membrane for 10 minutes at 1.2 amp/25 volts on the Trans-Blot Turbo Transfer System (Bio-Rad). HA-TUBA4A was detected via chemiluminescence using mouse HA antibodies (MMS-101R-200, Covance), goat anti-mouse HRP conjugate (sc-2005, Santa Cruz) and SuperSignal West Femto Maximum Sensitivity Substrate (Thermo Scientific).

HEK293 cell culture and immunofluorescence

HEK293T cells were maintained in DMEM supplemented with 10% fetal bovine serum, 100 units/ml penicillin and 100 µg/ml streptomycin at 5% CO_2. All reagents were purchased from Sigma-Aldrich. Transient transfections were performed in 6-well or 12-well plates using Lipofectamine 2000 (Life Technologies) according to the manufacturer's instructions. After 48-hour transfection, cells were processed for immunofluorescence analysis or protein solubility assay. For immunofluorescence, cells were fixed with 4% paraformaldehyde in phosphate buffered saline (PBS) at room temperature for 15 minutes, permeabilized with 0.2% Triton X-100 at room temperature for 5 minutes followed by blocking with 5% BSA in PBS at room temperature for 45 minutes. Incubation with primary antibodies (anti-HA, 1:100, Sigma-Aldrich anti-ubiquitin; 1:100, Life Technologies) was performed in blocking solution overnight at 4°C. The fluorescent-tagged secondary antibodies AlexaFluor 488 and AlexaFluor 594 (1:500, Jackson Immunoresearch) was used for detection. As a negative control, the primary antibody was replaced by normal goat serum. Slides were mounted with ProLong Gold antifade reagent containing DAPI to visualize the nuclei.

Quantification of Microtubule Incorporation

Quantification of HA-TUBA4A incorporation into microtubules was performed using imageJ. For each image, a region of interest (ROI) was selected for each HA-TUBA4A positive cell and the signal was thresholded to remove background noise. A circularity filter (circularity index ≥ 0.2) was then applied to the thresholded ROI to remove granular staining. The resulting image represented the filamentous HA staining. The ratio between the fluorescence intensities of the filtered cytoskeleton versus the thresholded ROI yielded an incorporation index ranging from 0 (no incorporation) to 1 (complete microtubule incorporation). The frequency distribution of these values was compared using the Kolmogorov-Smirnov test.

Microtubule Repolymerization Assay
COS7 cells were cultured in DMEM supplemented with 10% FBS (Life Technologies) and transfected with Lipofectamine 2000 (Life Technologies) accordingly to the manufacturer's recommendations. Thirty-six hours after transfection, cells were treated with 10μM nocodazole (Sigma-Aldrich) for 2 hours and allowed to recover in nocodazole-free medium for 0, 2.5, 5, 10, and 15 minutes before fixation with cold methanol.

Protein Fractionation and Insolubility assay
Protein fractionation was performed as previously reported with minor modifications(Koyama et al., 2006). Transfected HEK293T cells were collected in 300μl PBS buffer with protease inhibitors (Sigma-Aldrich) for each well of a 6-well culture plate. Samples were sonicated and centrifuged at 13,500xg for 10 minutes at 4°C. The supernatant was collected as the PBS-soluble fraction. The remaining pellet was sequentially resuspended in 150μl 1% Triton X-100, 5% SDS, and 8M urea, sonicated and centrifuged at 13,500xg for 10 minutes. All centrifugation steps were performed at 4°C, except for those with SDS, which were performed at room temperature to prevent precipitation. For the insolubility assay, transfected HEK293 cells were harvested with cold PBS with protease inhibitors, pelleted, resuspended in NP-40 lysis buffer (20mM Tris-HCl, pH 7.4, 1% NP-40, 150mM NaCl, 10% glycerol, 1mM DTT) containing proteasome inhibitors followed by sonication. Samples were incubated at 4^{o}C for 30 minutes, centrifuged, and the pellets washed with NP-40 lysis buffer and resuspended in urea-SDS buffer (NP-40 lysis buffer containing 8M urea, 3% SDS) followed by sonication. Proein fractions from both assays were run on a 10% polyacrylamide gel with equivalent volumes loaded per sample. Antibodies used: mouse HA (Cell Signaling Cat. No 2367) and IRDye 680 anti-mouse secondary antibody for detection (Li-Cor); rabbit GAPDH and rabbit Lamin (used as controls) and 800 anti-rabbit secondary antibody (Li-Cor).

Immunohistochemistry
Tissue from ALS cases and healthy controls was available from the MRC London Neurodegenerative Diseases Brain Bank. In brief, sections of 7μm thickness were cut from paraffin-embedded tissue blocks, then deparaffinised in xylene. Endogenous peroxidases were blocked by immersion in 2.5% H_2O_2 in methanol and immunohistochemistry performed. To enhance antigen retrieval sections were kept in citrate buffer (pH 6) for 10 minutes following microwave treatment. After blocking in normal swine serum (1:10, DAKO) in Tris-buffered saline (pH 7.6), anti-TUBA4A antibody (1:100, Cat.# AP13535b, Abgent) was applied overnight at 4°C. Following washes, sections were incubated with biotinylated secondary antibody (swine anti-rabbit, 1:100, DAKO, UK), followed by avidin:biotinylated enzyme complex (Vectastain Elite ABC kit, Vector Laboratories). Finally sections were incubated for 10-15 min with 0.5 mg/mL 3,3′-diaminobenzidine chromogen (Sigma-Aldrich) in TBS containing 0.05% H_2O_2. Sections were counterstained with Harris' haematoxylin and immuno-staining was analysed using a light microscope (Leica).

SUPPLEMENTAL TEXT

SLAGEN Consortium Members:

Sandra D'Alfonso[1], Letizia Mazzini[2], Giacomo P. Comi[3,4], Roberto Del Bo[3,4], Mauro Ceroni[5,6], Stella Gagliardi[5], Giorgia Querin[6], Cinzia Bertolin[6]

[1]Department of Medical Sciences, 'A. Avogadro' University of Eastern Piedmont, Novara, Italy.

[2]ALS Center, Department of Neurology, 'A. Avogadro' University of Eastern Piedmont, Novara, Italy.

[3]Neurology Unit, IRCCS Foundation Ca' Granda Ospedale Maggiore Policlinico, Milan 20122, Italy.

[4]Department of Pathophysiology and Transplantation, 'Dino Ferrari' Center - Università degli Studi di Milano, Milan 20122 Italy.

[5]Experimental Neurobiology Laboratory, IRCCS 'C. Mondino' National Neurological Institute, 27100 Pavia, Italy.

[6]Department of Neurosciences, University of Padova, Padova, Italy.

AUTHOR CONTRIBUTIONS

Sample Collection, Preparation and Clinical Evaluation: BNS, NT, ASG, ST, KPK, PK, CTi, CTr, SAS, AK, DC, VP, BC, JB, FB, ALtA, PCS, DMY, RLM, MP, JEP, JMB, MS, WvR, FPD, GL, SDU, SC, CCe, CL, GS, KEM, KLW, GAN, IPB, CLM, GAR, OH, JHV, LvB, AAC, HP, PJS, MRT, KT, FT, AGR, JDG, CG, AR, RHB, VS, CES, JEL, SLAGEN Consortium. Performed Experiments and Data Analysis: BNS, NT, CF, ASG, ST, JK, ELS, KPK, PK, JWM, CTi, EWD, CTr, CCo, SAS, EAL, AK, DC, BC, PCS, SA, WvR, JHV, FT, AGR, ZW, CG, AR, VS, CES, JEL. Scientific Planning and Direction: BNS, NT, CF, ASG, ST, JK, ELS, KPK, PK, CV, ZW, CG, AR, RHB, VS, CES, JEL. Initial Manuscript Preparation: BS, NT, CF, ASG, ST, ES, AR, VS, CES, JEL.

SUPPLEMENTAL REFERENCES

Chio, A., Calvo, A., Mazzini, L., Cantello, R., Mora, G., Moglia, C., Corrado, L., D'Alfonso, S., Majounie, E., Renton, A., et al. (2012). Extensive genetics of ALS: a population-based study in Italy. Neurology *79*, 1983–1989.

Dadd, T., Weale, M.E., and Lewis, C.M. (2009). A critical evaluation of genomic control methods for genetic association studies. Genet. Epidemiol. *33*, 290–298.

Fallini, C., Bassell, G.J., and Rossoll, W. (2010). High-efficiency transfection of cultured primary motor neurons to study protein localization, trafficking, and function. Mol Neurodegeneration *5*, 17.

Fallini, C., Bassell, G.J., and Rossoll, W. (2012). The ALS disease protein TDP-43 is actively transported in motor neuron axons and regulates axon outgrowth. Brain Research *1462*, 3703–3718.

Heinze, G., and Schemper, M. (2002). A solution to the problem of separation in logistic regression. Stat Med *21*, 2409–2419.

Johnston, C.A., Stanton, B.R., Turner, M.R., Gray, R., Blunt, A.H.-M., Butt, D., Ampong, M.-A., Shaw, C.E., Leigh, P.N., and Al-Chalabi, A. (2006). Amyotrophic lateral sclerosis in an urban setting: a population based study of inner city London. J. Neurol. *253*, 1642–1643.

Kenna, K.P., McLaughlin, R.L., Byrne, S., Elamin, M., Heverin, M., Kenny, E.M., Cormican, P., Morris, D.W., Donaghy, C.G., Bradley, D.G., et al. (2013). Delineating the genetic heterogeneity of ALS using targeted high-throughput sequencing. J. Med. Genet. *50*, 776–783.

Kiezun, A., Garimella, K., Do, R., Stitziel, N.O., Neale, B.M., McLaren, P.J., Gupta, N., Sklar, P., Sullivan, P.F., Moran, J.L., et al. (2012). Exome sequencing and the genetic basis of complex traits. Nat. Genet. *44*, 623–630.

Koyama, S., Arawaka, S., Chang-Hong, R., Wada, M., Kawanami, T., Kurita, K., Kato, M., Nagai, M., Aoki, M., Itoyama, Y., et al. (2006). Alteration of familial ALS-linked mutant SOD1 solubility with disease progression: its modulation by the proteasome and Hsp70. Biochem. Biophys. Res. Commun. *343*, 719–730.

Liu, J.S., Schubert, C.R., Fu, X., Fourniol, F.J., Jaiswal, J.K., Houdusse, A., Stultz, C.M., Moores, C.A., and Walsh, C.A. (2012). Molecular basis for specific regulation of neuronal kinesin-3 motors by doublecortin family proteins. Mol. Cell *47*, 707–721.

Oprea, G.E., Kröber, S., McWhorter, M.L., Rossoll, W., Müller, S., Krawczak, M., Bassell, G.J., Beattie, C.E., and Wirth, B. (2008). Plastin 3 is a protective modifier of autosomal recessive spinal muscular atrophy. Science *320*, 524–527.

Burden Test Results

Click here to download Supplemental Movies & Spreadsheets: BurdenTestResults.xls

Top Gene Variants

Click here to download Supplemental Movies & Spreadsheets: TopGeneVariants.xls